COOPERATION-INDUCED CRITICALITY IN NEURAL NETWORKS

Marzieh Zare, M.S.

Dissertation Prepared for the Degree of

DOCTOR OF PHILOSOPHY

UNIVERSITY OF NORTH TEXAS

August 2013

APPROVED:

Paolo Grigolini, Major Professor
Arkadii Krokhin, Committee Member
Guenter Gross, Committee Member
Jacek Kowalski, Committee Member
David Schultz, Chair of the Department of Physics
Mark Wardell, Dean of the Toulouse Graduate School

Zare, Marzieh. Cooperation-Induced Criticality in Neural Networks. Doctor of Philosophy (Physics), August 2013, 81 pp., 1 table, 28 illustrations, bibliography, 84 titles.

The human brain is considered to be the most complex and powerful information-processing device in the known universe. The fundamental concepts behind the physics of complex systems motivate scientists to investigate the human brain as a collective property emerging from the interaction of thousand agents. In this dissertation, I investigate the emergence of cooperation-induced properties in a system of interacting units.

I demonstrate that the neural network of my research generates a series of properties such as avalanche distribution in size and duration coinciding with the experimental results on neural networks both in vivo and in vitro. Focusing attention on temporal complexity and fractal index of the system, I discuss how to define an order parameter and phase transition. Criticality is assumed to correspond to the emergence of temporal complexity, interpreted as a manifestation of non-Poisson renewal dynamics. In addition, I study the transmission of information between two networks to confirm the criticality and discuss how the network topology changes over time in the light of Hebbian learning.

ACKNOWLEDGEMENTS

I am thankful to many people who made the completion of this work. I am thankful and indebted to my research supervisor Professor Paolo Grigolini for the excellent ideas, encouragement, and very extended patience. I thank my husband for his love, support and patience. I thank my parents and my siblings for the inspiration and untiring support. I also extend a warm gratitude to Professor Bruce J. West, Dr. Malgortaza Turalska and Dr. Nickolas Hollingshad for all the very informative discussions. I acknowledge the financial support from the Army Research Office and the Welch Foundation through grants N. B-1577 and W911NF-11-1-0478, respectively.

TABLE OF CONTENTS

Page

LIST OF TABLES

Page

LIST OF FIGURES

Page

CHAPTER 1

INTRODUCTION

A complex system is a system composed of interconnected units that as a whole exhibit a behavior not predictable from the behavior of the individual parts [1-2]. Few examples of these systems are ant colonies, human economies, social structures, and the human brain.

The human brain is considered as the most complex object in the known universe. The study of the brain and mind are inseparable [3]. The fundamental concepts behind the physics of complex systems motivated scientists to investigate the mind as a collective property emerging from the interaction of billions of agents [4]. The main concern is to understand cognition- its processes and its mechanisms at the level of molecules, neurons, networks of neurons, and cognitive modules [5].

In addition, scientists investigate how to define the collective behavior of neurons and how to explain animate behavior, decision making, and consciousness in the brain as a system governing the self-organization of large communities of locally interacting neurons [6]. Another key question to be answered is how information is transferred within the brain and between two brains as listener and speaker. The theoretical analysis and simulation help exploration of design parameters in wider ranges and in isolation, and help to understand the impact of each parameter on the observed behavior of the system.

There are different models defining the behavior of the neurons in the brain which aim for different computational purposes, while goals sometimes overlap. One of these models which used in this research is the leaky integrate-and-fire model [7]. This

model defines the global behavior of the neural system, making it a good candidate for using in study of the brain as a complex system.

Explaining the brain's overall behavior in terms of the underlying mechanism is a challenging problem, very difficult, if not impossible to solve. Some empirical results including avalanche analysis [8-9], dynamic range [10], information storage [11-13], information transmission [14-15] and computational power [16-19] suggest that the brain may work near criticality. Similar to other complex phenomena such as earthquakes, snow avalanches and forest fires, avalanches in neural networks are found to follow the popular scale-free distribution [20]. According to the popular view of Bak *et. al*. [6] criticality is realized spontaneously by complex systems rather than requiring the fine tuning of a control parameter with a critical value. They proposed the term self-organized criticality (SOC), as an operation of the system at criticality that generates the power law behavior in natural phenomena.

In this dissertation, cooperation is the key ingredient of the model that defines the interaction of units in the network. Cooperation-induced criticality has the effect of creating dynamical processes that the ordinary equilibrium statistical physics does not explain. The attention is focused on the criticality, and as is proposed by Werner [21], criticality and the renormalization group theory [22], the main theoretical tool to study criticality, play a fundamental role for the brain function and further theoretical advances in this direction may lead to viewing consciousness as a criticality-generated physical phenomenon.

This dissertation is organized as follows. Chapter 2 serves the purpose of introducing the mathematical concepts of the function defining the complexity in the

model, called Mittag-Leffler (ML) function and some of its properties. In chapter 3, the model defining the behavior of neural network of this research is discussed. Moreover, the network used throughout this manuscript is introduced and the cooperative behavior is theorized. Next, in chapter 4, we focus our attention on temporal complexity and fractal index of the system, an order parameter is suggested. It is shown that the system makes a transition from non-cooperative (random) state to a fully cooperative (periodic) state where complexity emerges in between. As a rigorous proof of criticality, the information transfer from one network to another is studied. The results show the maximal correlation and mutual information exist at criticality. Distribution of neural avalanches in size at criticality does not display power law scaling of 1.5, contradicting the widely shared conviction emerging from research on neural networks [8] while, coinciding with the few recent experiments on the real brain [23]. In chapter 5, It is shown that the emergence of the ML function is due to the low density of units in the that leads to the coexistence of complexity and periodicity. In chapter 6 two distinct form of survival probability truncation is discussed. Chapter 7 serves as the study of cooperation-induced topology of the network at criticality. Chapter 8 contains main conclusions and directions for future work.

CHAPTER 2

THE MITTAG–LEFFLER FUNCTION MODELS COOPERATION

This chapter is devoted to the introduction of the Mittag-Leffler (ML) function used throughout the entire manuscript to model the cooperation. Some discussions are brought to connect the distribution generated by the neural network of this research to the ML function. It is not intended as a comprehensive material about the ML function and serves only for the purpose of this research.

2.1 The Survival Probability as the Mittag-Leffler Function

The survival probability is defined as the chance that a target will survive a given operation. In complex systems perspective, survival is connected to the events generated in time. Throughout this manuscript, the main event of the neural system would be *neural firing*. Hence, the survival probability is the probability that a neuron does not fire for a time distance of t, written as $\Psi(t)$, and the time derivative of survival probability is waiting time distribution, $\psi(t)$, defined as $\psi(t) = -d\Psi(t) \,/\, dt$. Waiting time distribution is defined as

$$\psi(t) \propto \frac{1}{t^{\mu}} \tag{2.1}$$

and the corresponding survival probability reads as

$$\Psi(t) \equiv \int_{t}^{\infty} \psi(t')dt' \propto \frac{1}{t^{\mu-1}} \tag{2.2}$$

Now, let us examine how the ML function models relaxation of the survival probability of the neural network under study.

Metzler and Klafter [24] explain how the ML function established a compromise between two apparently conflicting complexity schools, the advocates of inverse power laws and the advocates of stretched exponential relaxation (see also West et al. [25]). We assign $\widehat{\Psi}(u)$ to the Laplace transform of survival probability, the following form (we adopt the notation for the Laplace transform $\widehat{\Psi}(u) \equiv \int_0^\infty dt\, \Psi(t) \exp(-ut)$)

$$\widehat{\Psi}(u) = \frac{1}{u + \lambda^\alpha (u + \Gamma_t)^{1-\alpha}} \tag{2.3}$$

With $\alpha < 1$. In the case, $\Gamma_t = 0$, this is the Laplace transform of the ML function [24], a generalization of the ordinary exponential relaxation which interpolates between the stretched exponential relaxation $exp(-(\lambda t)^\alpha)$, for $t < 1/\lambda$ and the inverse power law behavior $1/t^{\,\alpha}$, for $t > 1/\lambda$.

Recent work [26] has revealed the existence of quakes within the human brain, and proved that the time interval between two consecutive quakes is well described by a survival probability $\Psi(t)$, whose Laplace transform fits very well the prescription of Eq. 2.3. The parameter $\Gamma_t > 0$ has been introduced [26-27] to take into account the truncation thought to be a natural consequence of the finite size of the time series under study. As a matter of fact, when $1/\lambda$ is of the order of the time step and $1/\,\Gamma_t$ is much larger than the unit time step, the survival probability turns out to be virtually an inverse power law, whereas when $1/\lambda$ is of the order of $1/\,\Gamma_t$ and both are much larger than the unit time step, the survival probability turns out to be a stretched exponential function.

Failli et al. [27] illustrate the effect of establishing a cooperative interaction in the case of the random growth of surfaces. A growing surface is a set of growing columns whose height increases linearly in time with fluctuations that, in the absence of cooperation, would be of Poisson type. The effect of cooperative interaction is to turn

the Poisson fluctuations into complex fluctuations; the interval between two consecutive crossings of the mean value being described by an inverse power law waiting time distribution $\psi(t)$, corresponding to a survival probability, whose Laplace transform is given by Eq. 2.3.

In conclusion, according to the earlier work [27], we interpret $\alpha < 1$ as a manifestation of the cooperative nature of the process. In this research we illustrate a neural model where the time interval between two consecutive firings, in the absence of cooperation is described by an ordinary exponential function, thereby corresponding to $\alpha = 1$. The effect of cooperation is to make α decrease in a monotonic way, when increasing the cooperation strength, K, with no special critical value.

2.2 The Mittag-Leffler Function and Inverse Power Law

We note that Barabasi [28] stressed the emergence of the inverse power law behavior, properly truncated, as a consequence of the cooperative nature of human actions. Here we interpret the emergence of the ML function structure as an effect of the cooperation between neurons. The emergence of a stretched exponential function confirms this interpretation, if we adopt an intuitive explanation of it based on the distinction between the attempt to cooperate and to succeed. The action generator is assumed not to be fully successful, and a success rate parameter $P_S < 1$ is introduced with the limiting condition $P_S = 1$ corresponding to full success.

To turn this perspective into a theory, yielding the theoretical prediction of Eq. 2.3, we assume that the time interval between two consecutive cooperative actions is described by the function $\psi^S(\tau)$, where the superscript (S) indicates that from a formal

point of view we realize a process corresponding to subordination theory [29-32]. Here we make the assumption that the survival probability for an action, namely the probability that no action occurs up to a time t after an earlier action has the form

$$\Psi^S(t) = \left(\frac{T_S}{t + T_s}\right)^{\alpha} \tag{2.4}$$

With $\alpha = \mu_s - 1$ and $\mu_s < 2$. As a consequence, the time interval between two consecutive actions has the distribution density $\psi^S(\tau)$ of the form

$$\psi^S(\tau) = (\mu_S - 1)\frac{T_S^{\mu_S - 1}}{(\tau + T_S)^{\mu_S}} \tag{2.5}$$

Note that the distance between two actions is assumed to depart from the condition of ordinary ergodic statistical mechanics. In fact, the mean time distance τ between two consecutive actions emerging from the distribution density of Eq .2.5 is

$$\langle\tau\rangle = \frac{T_S}{\mu_S - 2} \tag{2.6}$$

For $\mu_S > 2$. For $\mu_S < 2$, Eq. 2.6 diverges. As a consequence this process shares the same non-ergodic properties as those generated by human action [28].

It is evident that when $P_S = 1$ the survival probability $\Psi(t)$ is equal to $\Psi^S(t) = \int_t^{\infty} \psi^S\,(t')dt'$. When $P_S < 1$, from Appendix A using the formalism of the subordination approach [26-27,29], we easily prove that the Laplace transform of $\Psi(t)$ is given by

$$\widehat{\Psi}(u) = \frac{1}{u + P_S\widehat{\Phi}(u)} \tag{2.7}$$

Where

$$\widehat{\Phi}(u) = \frac{u\hat{\psi}^S(u)}{1 - \hat{\psi}^S(u)} \tag{2.8}$$

To prove the emergence of the ML function of Eq. 2.3 with $\Gamma_t = 0$, from this approach, let us consider for simplicity's sake the case where $\psi^S(\tau)$ is not truncated. In the non-ergodic case, using the Laplace transform method [25], we obtain that the limiting condition yields Eq. 2.3 with

$$\lambda = \left(\frac{P_S}{\Gamma(1-\alpha)}\frac{1}{T_S^\alpha}\right)^{1/\alpha} \tag{2.9}$$

where $\Gamma(1-\alpha)$ is the Gamma function. Note that when $P_S = 1$, the Laplace transform of Eq. 2.7 in the limit of $u \to 0$ coincides, as it must, with the Laplace transform of $\Psi^S(t)$. In conclusion, we obtain

$$\hat{\Psi}(u) = \frac{1}{u + \lambda^\alpha u^{1-\alpha}} \tag{2.10}$$

With $\lambda^\alpha \propto P_S$. In the neural model of this research, we define a parameter of cooperation effort, denoted by the symbol K. The success of cooperation effort is measured by the quantity

$$g(K) = \lambda(K)^{\alpha(K)} \tag{2.11}$$

We determine that the sign of success is given by the number of neurons firing at the same time.

In the next chapters, it is explained how to establish a connection between the ML function introduced here and the cooperation-induced criticality of the neural network under study.

CHAPTER 3

MODEL DESCRIPTION

This chapter serves as a description of the system of cooperating neurons in the leaky integrates-and-fire model. First, a system of fully synchronized neurons is introduced; next, a modified version of this model, which is the core model of this manuscript, is studied. It is shown that the neural system of this study generates neural avalanches in size and time comparable to the empirical results on neural networks both in vivo and in vitro.

3.1 The Mirollo-Strogatz Model

Neuronal synchronization was found to be the main source of neuronal avalanches, while the theoretical foundation of these processes is still open [33]. A neuronal avalanche is a cascade of bursts of activity in neuronal networks whose size distribution can be approximated by a power law, as in critical sandpile model [6]. Neuronal avalanches were observed in cultured and acute cortical slices [8].

A model of synchronization of pulse-coupled oscillators was studied based on Peskin's model [34]. The main purpose of studying this model was self-synchronization of the cardiac pacemaker by Mirollo and Strogatz [35]. The model is a network of N integrate-and-fire neurons. The equation of motion of each neuron follows

$$\frac{dx_i}{dt} = -\gamma x_i + S \qquad\qquad i = 1, \dots, N \qquad\qquad (3.1)$$

where x_i denotes the neuron potential, $1/\gamma$ is a constant governing the decay of the voltage back to the resting level and S is a positive constant making the potential essentially increase with time. When x_i reaches the threshold value Θ, it fires and

instantly sets to zero, $x_i = 0$. We can find the trajectory of each neuron; assuming $\tilde{x}(t) = x - \frac{S}{\gamma}$, and setting $x(0) = 0$, we get

$$x_i(t) = \frac{S}{\gamma}(1 - e^{-\gamma t}) \tag{3.2}$$

For simplicity, the threshold is defined as $\Theta = 1$, hence the time for a single neuron to reach the threshold is given by

$$T_{MS} = \frac{1}{\gamma}\ln\left(\frac{1}{1 - \frac{\gamma}{S}}\right) \tag{3.3}$$

in which $S > \gamma$ forces each neuron to move positively toward the threshold. The spiking pattern of this model is shown in Panel a of Fig. 3.1; as is seen from the figure, all neurons synchronize after a period of time around the value predicted by Eq. 3.3. The trajectory of a single neuron corresponding to Eq. 3.2 is shown in Panel b of Fig. 3.1, the single neuron moves toward the threshold with the period of Eq. 3.3.

Here, the case in which all neurons interact with each other, or in other words, cooperate through pulse-coupling is considered, and is called All-To-All (ATA). When one neuron fires all the others are pulled up by a value K which is called cooperation strength or coupling. With this model, Mirollo and Strogatz proved that over a long enough observation time all neurons would synchronize with the period of Eq. 3.3. This gives us the waiting time distribution of time distances between two consecutive firing as

$$\psi(\tau) = \delta(\tau - T_{MS}) \tag{3.4}$$

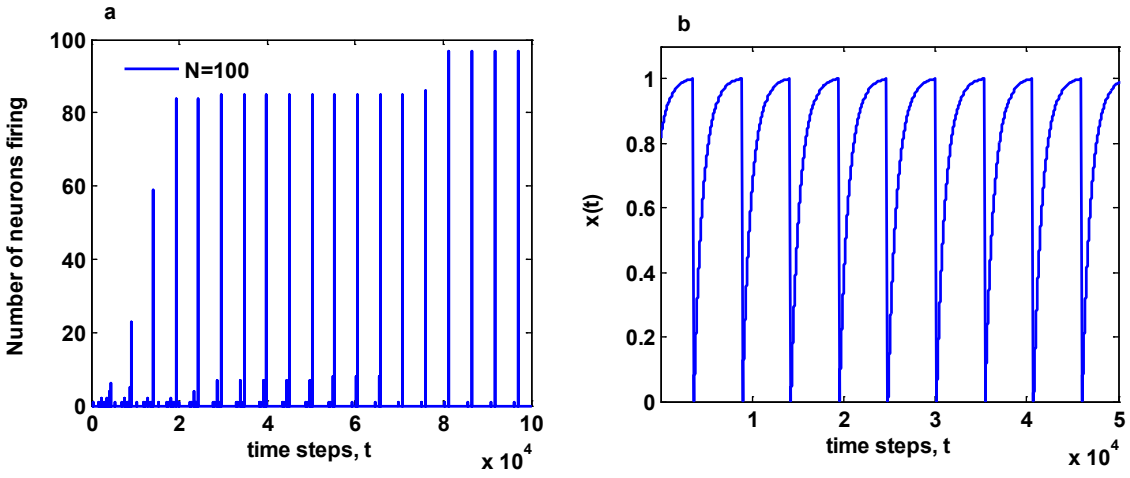

Fig. 3.1. Illustration of the Mirollo-Strogatz synchronization. Spiking pattern of a system of neurons in ATA network. After a while all neurons synchronize (a). Trajectory of a single neuron is depicted; neuron starts from a random value or zero, and reaches the threshold which is set to 1(b).

3.2 Stochastic Version of the Mirollo-Strogatz Model

Due to the deterministic nature of the Mirollo-Strogatz neuron model leading to the waiting times distribution of Eq. 3.4, this model is clearly unrealistic with no complexity. To make it more realistic and to generate complexity as well, it is appropriate to replace Eq. 3.1 with the stochastic equation as suggested by the authors of Ref. [36] as:

$$\frac{dx_i}{dt} = -\gamma x_i + S + \xi(t) \qquad i = 1, \dots N \qquad (3.5)$$

Here, $\xi(t)$ is a Gaussian random fluctuation as

$$< \xi(t)\xi(t') >= \sigma^2 \delta(|t - t'|) \qquad (3.6)$$

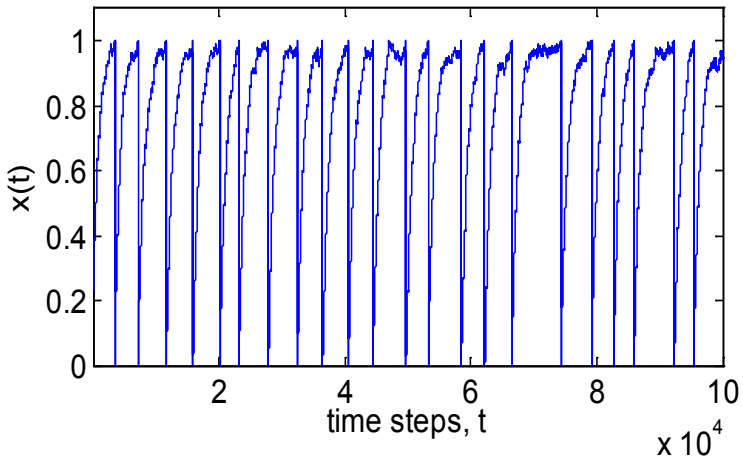

Fig. 3.2. The Potential of a single neuron in time in the presence of noise. The noise has the effect of making the behavior stochastic; neuron fire earlier or later than the period of Eq. 3.3.

The addition of noise has the effect of changing the firing of a single neuron into stochastic pattern of activity as if it may fire earlier or later than T_{MS} (See Fig. 3.2). With the same treatment as that of the Mirollo-Strogatz model, when one neuron fires all the neurons connected to it are pulled up by a value of K which is the cooperation parameter. In order to make it more clear, Eq. 3.5 with considering noise and cooperation may be written as

$$\frac{dx_i}{dt} = -\gamma x_i + S + \xi(t) + K\sum_{j=1}^{N} a_j \Lambda_{ij}\delta\left(t - t_j - t_d\right) \qquad i,j = 1,\dots N \qquad (3.7)$$

in which a_i refers to the excitatory connection if $a_i = 1$ or inhibitory connection if $a_j = -1$; Λ_{ij} is element of an adjacency matrix[1] defining connection of neuron i to neuron j; t

[1] Adjacency matrix is a matrix that defines the connection between neurons in a network. This matrix is of size NxN, where N is the number of neurons in the network. If for example, neuron 1 is connected to neuron 2, then $\Lambda_{ij} = 1$, otherwise $\Lambda_{ij} = 0$. The symmetric adjacency matrix is used to define the directed connections, which is the type of connection that we use here. If the connections are indirect, the adjacency matrix is asymmetric.

is the time of realization; t_j is the time of firing of neuron j, here is ($t_j = t$); and t_d is the time lag of firing neuron from the time of receiving the cooperation.

For the sake of simplicity, the time lag of cooperation is set to zero. The results, not shown here, of considering delay time proportional to the distance of neurons in the network shows no significant change in the nature of complexity that is the interest of this research. In the numerical calculations of this research, we adopt two different initial conditions: the former is based on assigning $x_0 = 0$ to all neurons at the rest state and in the latter condition x_0 is a random numbers between 0 and 1. In Chap.4, we will discuss that the correlation and mutual information between two networks depends on the initial condition of x.

Considering Eq. 3.5, there are two possible discussions on the stochastic version of the Mirollo-Strogatz; Eq. 3.5, i) $\gamma = 0$ and ii) $S = 0$. The former is called *perfect integrator*. The waiting time distribution, $\psi(\tau)$ in this case, can be solved using the first passage time formalism. Hence, Eq. 3.5 may be written as

$$\frac{dx}{dt} = S + \xi(t) \tag{3.8}$$

The Fokker-Planck equation reads as [37]

$$\frac{\partial}{\partial t}p(x,t/x_0) = \left(-S\frac{\partial}{\partial x} + D\frac{\partial^2}{\partial x^2}\right)p(x,t/x_0) \tag{3.9}$$

$p(x,t/x_0)$ is the probability of finding the particle at position x at time t, D is the diffusion coefficient, and $x_0$is the initial position of the particle. Setting the threshold at $x_0 = \Theta$, so to speak, the system is prepared at the threshold; the solution of Eq. 3.9 is written as

$$p(x,t/\Theta) = \frac{1}{(4\pi Dt)^{1/2}}exp\left(-\frac{(x-\Theta-St)^2}{4Dt}\right) \tag{3.10}$$

To find the waiting time distribution, $\psi(\tau)$, the relation below is used

$$p(x,t/x_0) = \int_0^t d\tau\psi(\tau)\, p\left(x, t - \frac{\tau}{\Theta}\right) \tag{3.11}$$

From Appendix B, we obtain

$$\psi(t) = \frac{(\Theta - x_0)}{(4\pi D t^3)^{\frac{1}{2}}} exp\left(-\frac{(\Theta - x_0 - St)^2}{4Dt}\right) \tag{3.12}$$

Then substituting $x_0 = 0,\ \Theta = 1$, and $D = \sigma^2$, we arrive at

$$\psi(t) = \frac{1}{(4\pi D t^3)^{\frac{1}{2}}} exp\left(-\frac{(1 - St)^2}{4\sigma^2 t}\right) \tag{3.13}$$

The waiting time distribution of Eq. 3.13 was originally found by Mandelbrot [38]. This distribution is plotted in Fig. 3.3. Upon increase of noise, there is a shifting of the peak to the left thereby producing a slow tail that is proportional to $1/t^{\mu}$ with $\mu = 1.5$. However, the tail is truncated and for $t \to \infty$ we have

$$\psi(t) \propto \frac{1}{t^{1.5}} exp\left(-\left(\frac{S}{\sigma}\right)^2 \frac{t}{4}\right) \tag{3.14}$$

For further reading, see Ref.[38].

In the neural system under study, setting $\gamma = 0$ in Eq. 3.3, we get $T_{MS} \approx 1/S$, thereby simplifying the numerical calculations. It seems that many neurophysiologists believe that $\gamma > 0$ makes the neural model more realistic. In this study the choice of $\gamma > 0$ is not essential and the main reason behind the adoption of that is because the Mirollo-Strogatz model [35] rests on this condition.

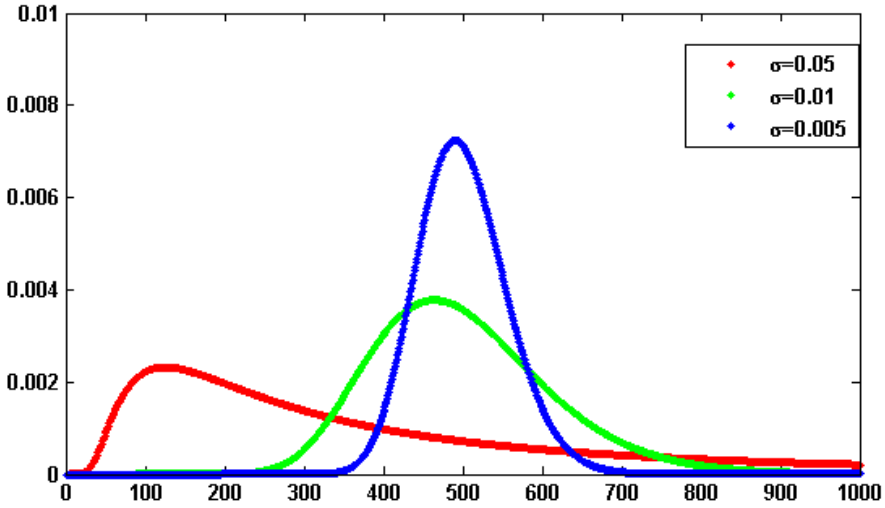

Fig. 3.3. Illustration of the analytical solution of the perfect integrator. Increasing the noise intensity has the effect of broadening the waiting time distribution and shifting the peak to the left.

To the best of our knowledge, there is still no analytical solution for $\gamma > 0$. We have numerically evaluated the waiting time distribution of a single neuron in the system of interacting neurons for different values of noise. As shown in Fig. 3.3, noise has the effect of widening the waiting time distribution and shifting the peak to the left. For our numerical purposes, we adopted $S = 0.001005$ and $\gamma = 0.001$. The choice of a proper value for the noise rests on the analytical discussion of perfect integrator. In fact, this value is chosen as if the waiting time distribution peaks at T_{MS}. With this choice, we can make sure that the value of noise in the system is enough to make the system stochastic and lose its initial condition to perceive the cooperative behavior. The arrow in Fig. 3.4 indicates the period of Eq. 3.3, T_{MS}, and as is seen, the waiting time distribution is maximized at this time for $\sigma = 0.0001$.

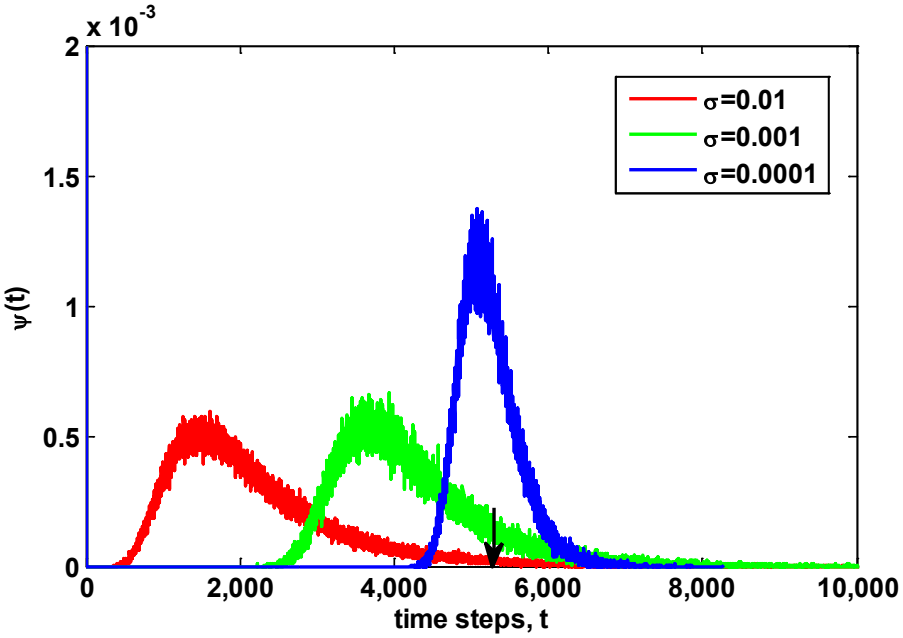

Fig. 3.4. Numerical calculation of the waiting time distribution of a single neuron for different noise intensities. Similar to analytical counterpart, increasing the noise intensity has the effect of shifting the peak to the left and widening the distribution. The peak should correspond to the given time of Eq. 3.3, here is 5300.

This value of the noise is used throughout the numerical calculations of this manuscript.

Another possible analytical discussion is $S = 0$, called overdamped oscillator. In this case Eq. 3.5 becomes

$$\frac{dx_i}{dt} = -\gamma x_i + \xi(t) \qquad i = 1, \dots N \tag{3.15}$$

This is identical to Kramers problem [39]. In the neural system, we choose $S > \gamma > 0$ in order to force neurons move positively toward the threshold in order to make the model behave as real neurons. Hence, the case of $S = 0$ does not apply on the neural model of this research and this case was only mentioned to complete the analytical discussion of this section.

3.3 Neurons Cooperative Behavior

The cooperative properties of the networks are determined as follows. Each neuron is the node of a network and interacts with all the other nodes linked to it. When a neuron fires all the neurons linked to it make an abrupt step ahead by a value of K. This is the cooperation parameter, or coupling strength. An inhibition link may be introduced by assuming that when one neuron fires all the other neurons linked to it make a step backward through inhibition links. This model is richly structured and may allow us to study a variety of interesting conditions.

There is widespread conviction that the efficiency of a network, namely its capacity to establish global cooperative effects, depends on network topology, as suggested by the brain behavior [26,40]. The link distribution itself, rather than being fixed in time, may change according to the Hebbian learning principle [41]. It is expected that such learning generates a scale-free distribution [40], thereby shedding light on the interesting issue of burst leaders [42]. These properties are studied in this research.

Herein, we focus on cooperation by assuming that all the links are excitatory. To further emphasize the role of cooperation, the ATA assumption adopted by Mirollo and Strogatz [35] was studied in an earlier work [43]. In spite of the fact that the efficiency of the ATA model is reduced by the action of the stochastic force $\zeta(t)$ that weakens the action of cooperation, thereby generating time complexity, the ATA condition generates the maximal efficiency and neuronal avalanches. However, this condition inhibits the realization of an important aspect of cooperation, namely, locality breakdown. For this reason, herein, we also study the case of a regular lattice, two-dimensional (2D)

network, where each node has four nearest neighbors and consequently four links (configuration of the network is shown in Fig. 3.5).

It is important to stress that to make our model as realistic as possible, we can introduce a delay time between the firing of a neuron and the abrupt step ahead of all its nearest neighbors. This delay is assumed to be proportional to the Euclidean distance between the two neurons, and it is expected to be a property of great importance to prove the breakdown of locality when the scale-free condition is adopted. As mentioned before, the simplified conditions studied in this research would not be affected by a time delay that should be the same for all the links. For this reason, we do not further consider time delay.

For the cooperation strength we must assume the condition $K \ll 1$. When K is of the order of magnitude of the potential threshold $\Theta = 1$, the collective nature of cooperation is lost because the firing of a few neurons causes an abrupt cascade in which all the other neurons fire. Thus, we do not consider the non-monotonic behavior of network efficiency to be important that our numerical calculations show to emerge by assigning K values of the same order as the potential threshold.

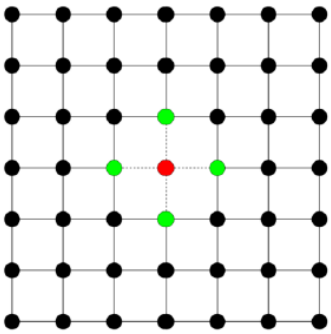

Fig. 3.5. Configuration of the regular lattice under study. Single node and its four nearest neighbors with whom it interacts are marked.

We also note that in the case of this model the breakdown of the ML structure, at large times, is not caused by a lack of cooperation, but by the excess of cooperation. To shed light on this fact, keep in mind that this model has been solved exactly by Mirollo and Strogatz when $\sigma = 0$ [35]. In this case, even if we adopt initial random conditions, after a few steps, all the neurons fire at the same time, and the time distance between two consecutive firings is given by Eq. 3.3. As an effect of noise the neurons can also fire at the same times, and consequently, setting $\sigma > 0$, a new, and much shorter time scale is generated. When we refer to this as the time scale of interest, the Mirollo and Strogatz time T_{MS}, plays the role of a truncation time and

$$\Gamma_t \approx \frac{1}{T_{MS}} \tag{3.16}$$

To examine this condition, let us assign to K a value very close to $K = 0$. In this case even if we assign to all the neurons the same initial condition, $x = 0$, due to the presence of stochastic fluctuations the neurons fire at different times thereby creating a spreading on the initial condition that tends to increase in time, even if initially the firing occurs mainly at times $t = nT_{MS}$. The network eventually reaches a stationary condition with a constant firing rate G given by

$$G = \frac{N}{\langle \tau \rangle} \tag{3.17}$$

Where $\langle \tau \rangle$ denotes the mean time between two consecutive firings of the same neuron. For $\sigma \ll 1$, $\langle \tau \rangle = T_{MS}$. From the condition of a constant rate G, we immediately derive the Poisson waiting time distribution

$$\psi(\tau) = Ge^{-G\tau} \tag{3.18}$$

Consequently, this heuristic argument agrees very well with numerical results. We consider a set of N identical neurons, each of which obey Eq. 3.5 and we also assume, with Mirollo and Strogatz [35], that the neurons cooperate. For the numerical simulation we select the condition

$$G \ll 1 \ll N \ll T_{MS} \tag{3.19}$$

yielding

$$\frac{1}{G} \approx \frac{T_{MS}}{N} \ll T_{MS} \tag{3.20}$$

thereby realizing the earlier mentioned time scale separation. It is evident that this condition of non-interacting neuron fits Eq. 2.3 with $\alpha = 1$ and

$$\lambda(K = 0) = G \tag{3.21}$$

In this case, the time truncation is not perceived, due to the condition $1/G \ll T_{MS}$. In the next chapter numerical results will show more details about the effect of cooperation.

As far as the ML time complexity is concerned, we adopt the same fitting procedure as that used in Ref.[43]. We evaluate the Laplace transform of the experimental $\Psi(t)$ and use as a fitting formula Eq. 2.3 with $\Gamma_t = 0$, to find the parameter α. Then we fit the short-time region with the stretched exponential

$$\Psi(t) = exp(-(\lambda t)^{\alpha}) \tag{3.22}$$

To find λ. We determine that in the regular lattice condition as in the ATA condition [43], activation of cooperation has the effect of generating the ML time complexity. From the numerical results of the next chapter on fitting parameter of the ML function, we see that any non-vanishing value of K turns the Poisson condition $\alpha = 1$ into the ML temporal complexity $\alpha < 1$. We have assessed numerically $\langle\tau\rangle$=5300, using Eq. 3.18, $G = 0.0189$ and $T_{MS} = 5303.3$. In the case of no interaction, the probability that two neurons fire at

the same time is G^2. Due to $G \ll 1$, the simultaneous firing of two neurons is almost impossible and the survival probability is exponential signaling a Poisson process.

We shall see that survival probability makes a transition from Poissonian to non-Poissonian process. An order parameter is suggested based on the phase transition gained from temporal complexity. As the result of cooperation, system shows interesting properties such as locality breakdown and long-rang correlation.

CHAPTER 4

COOPERATION-INDUCED CRITICALITY IN REGULAR LATTICE

In this chapter, numerical calculations on the regular lattice are discussed. We start with spiking pattern of the neural network and survival probability distribution to define the temporal complexity. Temporal complexity suggests a critical point at which the phase transition occurs. To confirm the critical value, renewal properties and transmission of information is studied. Finally the self-organization criticality hallmark, avalanche distribution in time and size, are discussed to see if the system displays the crucial exponents of 1.5 in size [8] and 2 in time duration [8] at criticality.

4.1 Spiking Pattern and Survival Probability

Spiking pattern is the most important output of a neural system, which indicates the cumulative number of spikes per unit of time. In practice, neurophysiologists record the spiking pattern and analyze them to understand the system's behavior whether it is a living rat brain cultured on Microelectrode array[2] or an Electroencephalography EEG [3] pattern of a living brain. In this research, we also follow the same procedure which is in fact in line with our approach of studying temporal complexity. We make a distribution out of time series, which is the normal distribution, here called waiting time distribution Eq. 2.1 Followed by that, we calculate the corresponding cumulative distribution using Eq. 2.2.

[2]Microelectrode arrays are substrates of integrated thin film conductors terminating in exposed recording sites through which neural signals are obtained or delivered, essentially serving as neural interfaces that connect neurons to electronic circuitry [44].

[3] Electroencephalography (EEG) is the recording of electrical activity along the scalp. EEG measures voltage fluctuations resulting from ionic summations of millions of neuronal currents within the neurons of the brain [45].

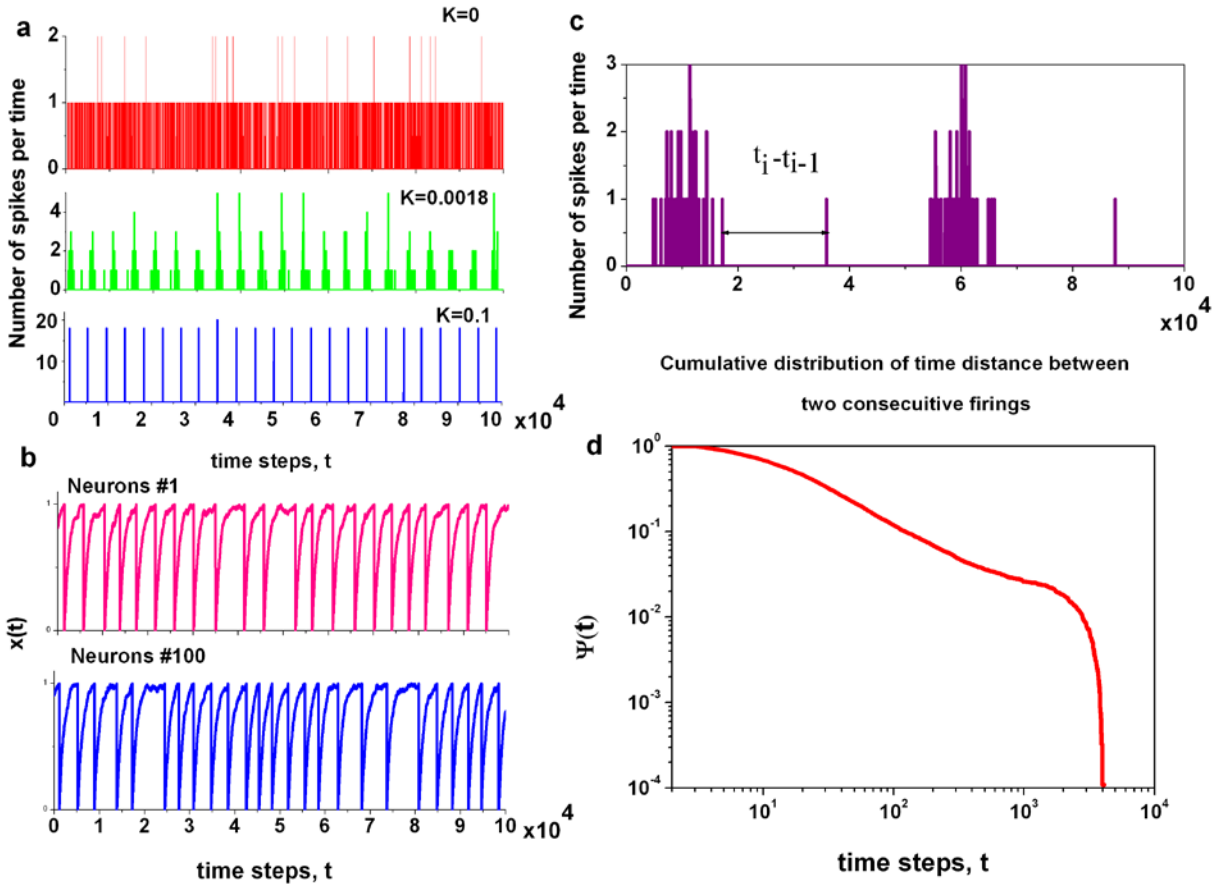

Fig. 4.1. Illustration of the data collection and analysis of the neural network under study. Spiking pattern for three different cooperation parameters is shown; increasing the cooperation makes neurons fire at the same time until they synchronize (a) trajectories of two random neurons (b), close view of a spiking pattern (c), survival probability gained from Panel c (d).

Fig. 4.1 plots the procedure of data collection and analysis from regular lattice. Panel a represents the spiking pattern for different values of cooperation parameter, or coupling in the system. As is seen from the figure, increasing the value of cooperation

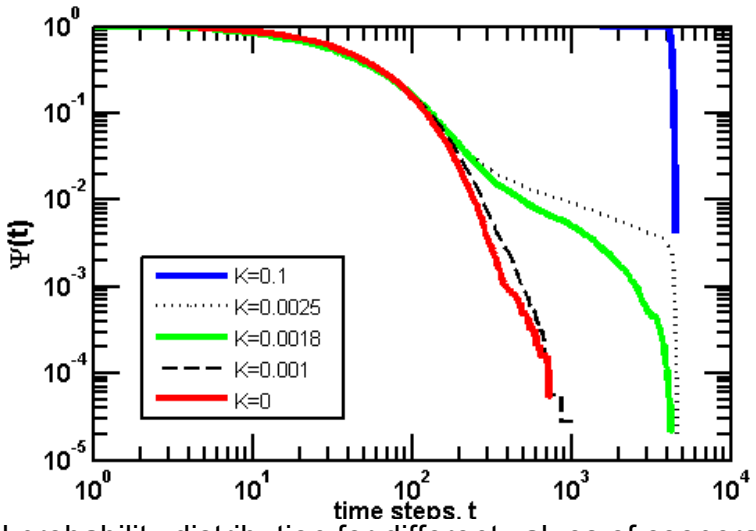

Fig. 4.2. Survival probability distribution for different values of cooperation in the regular lattice. Due to increasing the cooperation, that results in the increment of time distance between two consecutive firings survival probability decays slower.

leads to the burst formation until the value of cooperation is too large that it makes the pattern totally periodic. Panel b shows the trajectory of two random neurons. Panel c is a close view of a spiking pattern that indicates visually how we evaluate the time distance between two consecutive firings and find the cumulative distribution shown in Panel d of Fig. 4.1.

If we evaluate the survival probability for three spiking patterns of Panel a of Fig. 4.1 and two other cooperation parameters, $K = 0.001$ as dashed line, and $K = 0.0025$ as dotted line, we gain the plots shown in Fig. 4.2. These curves are the central results of a bunch of unshown curves for different values of cooperation parameter, *K*. Survival probability distributions indicate the following: Increment of coupling in the neural network extends the time distance between two consecutive firings, and as a consequence of extension of time distances, the survival probability distribution decays slower. If the cooperation is very large, all neurons fire together and make the waiting time distribution follow Eq. 3.3, and finally, survival probability distribution will look like

blue line of Fig. 4.2. We refer to this behavior as a transition from Poisson process to the ML dynamics and finally a breakdown of the ML function. More details will be discussed in the following sections which are devoted to description of criticality, and phase transition.

4.2 Detection of Temporal Complexity

The mathematical concept of the ML function in Chap.2 was discussed. Therein, it was explained that the ML function models the cooperation. As we see from Fig. 4.3, two distinctive time regimes characterize the survival probability: short time and long time regimes that can be fitted by stretched exponential $exp(-(\lambda t)^{\alpha})$ with $\alpha < 1$ and inverse power law $1/t^{\alpha}$ respectively.

Fitting parameters, α and λ can be found under a fitting procedure. α indicates the power law exponent of survival probability holding $0 < \alpha < 1$, and λ indicates the scale of the stretched exponential of survival probability distribution. The procedure is shown in Fig. 4.3. This fitting procedure is accomplished on each time regime in two steps: fitting of the stretched exponential and fitting of the inverse power law. However, fitting on the Laplace transformation of survival probability can be done in a single step on the total observation time. It is important to note that the fitting parameters found in both cases are equal.

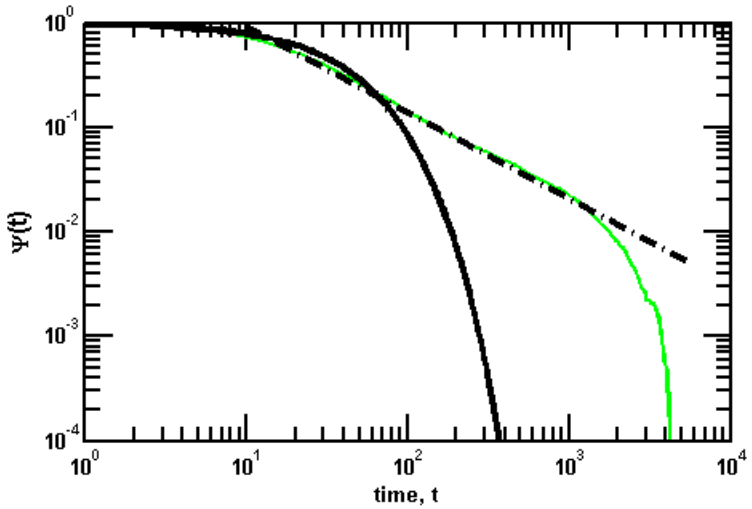

Fig. 4.3. Fitting procedure on survival probability in time representation for $K = 0.0018$. black curve is an ordinary exponential fitted on the short time regime of the ML function with $\alpha = 0.75$ and $\lambda = 0.034$. Black line is an inverse power law fitted on the long time of the ML function with $\alpha = 0.75$. The fitting parameter α has to be equal in both fittings as a condition of accurate procedure.

Hence, it is more convenient to use the Laplace transform of survival probability and find the fitting parameters. In order to do this fitting, a procedure is done as follows:

1. Apply a Laplace transform on survival probability gained from neural dynamics.
2. Fit the data given in step 1 into Eq. 2.6 to find α and λ.
3. Repeat the procedure for different values of K.
4. Plot α , λ ,and λ^{α} versus K to see how the fitting parameters of survival probabilities are changing with increasing the coupling.

As an example, for a value of $K = 0.0018$, step 1 and 2 are executed; the Laplace transform of survival is calculated and the fitting parameters are found, as is illustrated in Fig. 4.4. The Laplace transform of u is $1/t$. The parameter u is chosen to hold $\varepsilon < u < 0.1$; the lower and upper limits of this condition are set to cover the long time and short time regime respectively. The choice of the lower limit, ε, depends on the

natural time of the system-herein the system's truncation time, T_{MS}- Hence , $u_{low} \approx 1/\, T_{MS}$.

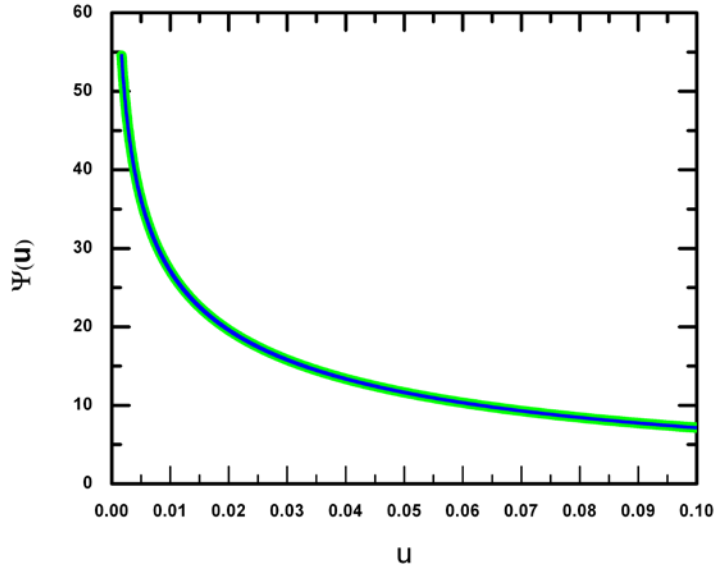

Fig. 4.4. Laplace transform of survival probability, $\Psi(u)$. The transformation is done in two different ways as shown in this plot: numerical and analytical. Numerical transformation is done applying the numerical Laplace transform on data of survival probabilities in time. The analytical was done by fitting the fitting parameters α and λ into Eq. 2.6.

The upper limit is set in order to hold this condition: due to the discrete time, we need to make sure that the short time is fully covered thus $t >> 1$, consequently $t \approx 10$ and $u_{upp} = 0.1$. Finally, step 4 of the procedure is executed, which is repeating the fitting procedure on the Laplace transform of survival probability distribution for a wide range of cooperation parameters. Then α, λ, and λ^{α} are plotted versus K. The results of this step are sketched in Fig. 4.5.

The numerical results suggest the following interpretation: In the ideal case of a large number of interacting units, $\alpha = 1$ for $0 \leq K \leq K_C$ and the stretched exponential $exp(-(\lambda t)^{a})$, is an ordinary exponential with $\lambda = G$, (see Eq. 3.18 and Eq. 3.22). At $K = K_C$, the value of α drops to a value smaller than 1 see Panel a of Fig. 4.5.

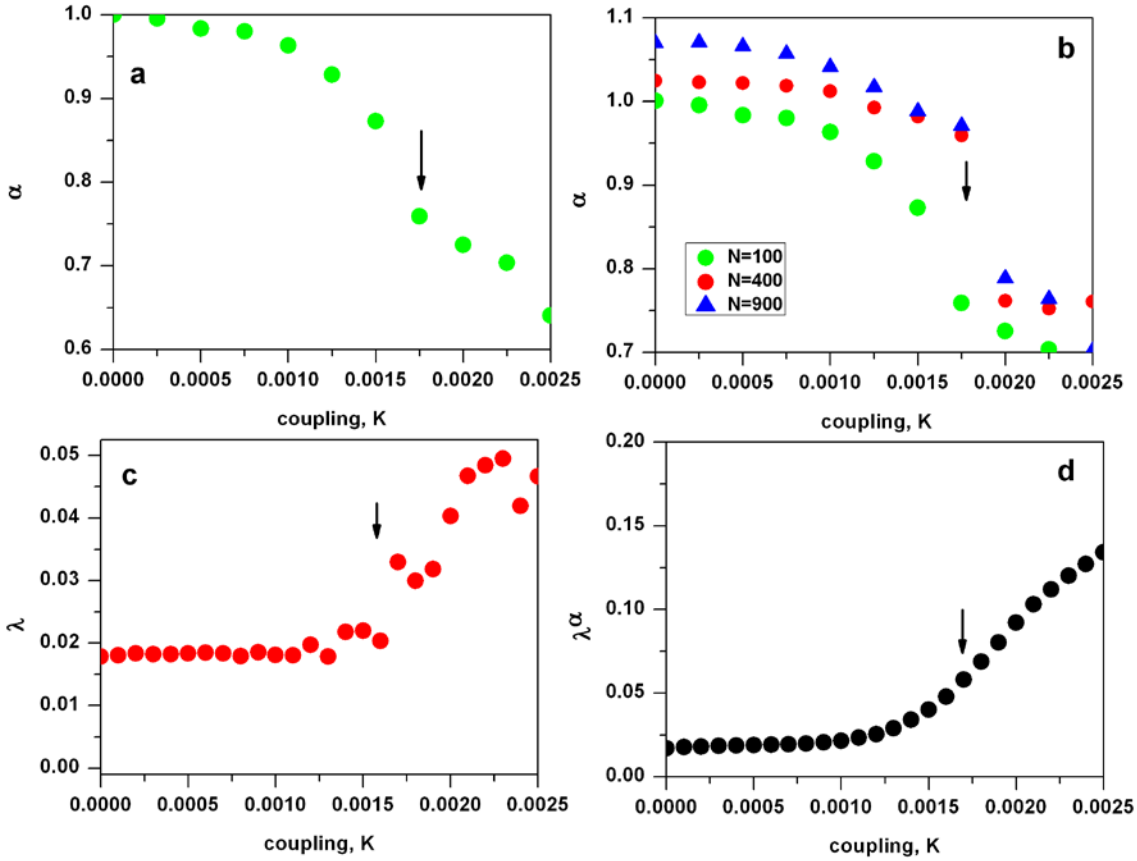

Fig. 4.5. Fitting parameters of survival probabilities in the regular lattice. a) The changes of power index with cooperation parameter. Notice the change in the steepness of descent near ≈ 0.0018 . b) The changes of power law index for systems of larger size are compared with the results of Panel a. As is obvious the abrupt change is more obvious when the size increases. c) Scale of stretched exponential, λ notice the abrupt change in $K \approx 0.0018$. d) λ^{α} or $g(k)$ according to Eq. 2.11 measures the success of an effort, the change at the same value of K is considerable.

The results of Panel b shows that the decrease of α becomes more pronounced with increasing N. We ran the model on the larger system of $N = 400$, a square lattice of size $L = 20$ and also $N = 900$, a square lattice of size $L = 30$. The results suggest that for a very large number of interacting units, α may drop to $\alpha_C \approx 0.75$, which corresponds to

$$K_C \approx 0.0018 \tag{4.1}$$

We interpret the steepness of changes as criticality. Panel a of Fig. 4.5. suggests a first order phase transition. λ and λ^{α} also show abrupt change at the same value of cooperation parameter as is seen in Fig. 4.5.

4.3 Phase Transition

We have already shown in the previous section that the abrupt change in the fitting parameters might correspond to a critical value. In order to explore more in detail where the transition occurs, we need to determine the type of phase transition taking place here and discuss how to define an order parameter to find the critical value. The numerical results of the earlier work of our group [42,45] have established that cooperation is perceived immediately with a finite value of cooperation parameter K of even extremely small intensity. This led these authors to make the conjecture that this neural model may be a manifestation of the extended criticality advocated by Longo et.al [46]. [4]

Due to the action of a finite number, we propose a somewhat different interpretation based on the observation of the well known second-order phase transition.[5] We cannot determine the critical value of K_C, by using, for instance, the method of Binder's cumulants [48] because this method is usually applied to Ising-like phase transitions, see for instance [49]. Here, though, the transition to cooperation does not seem to be an ordinary second-order phase transition. Using the parameter, $g(k)$

[4]In biology, the "coherent critical structures" are "extended" and organized in such a way that they persist in space and time. So there is not a single critical point but there is a wide range of critical values.

[5]*Second-order phase transitions* are continuous in the first derivative (the order parameter, which is the first derivative of the free energy with respect to the external field, is continuous across the transition) but exhibit discontinuity in a second derivative of the free energy [47].

that measures the success of an effort of the system to inter the cooperative regime, we define the order parameter of this process by means of $\Gamma(K)$ by

$$\Gamma(K) = \int_0^K dk\, \lambda^{\alpha} \tag{4.2}$$

This parameter is plotted in Fig. 4.6. The numerical result of Fig. 4.6 is qualitatively a function of control parameter, similar to the mean field of the Ising-like model of Ref.[49]. However, the nature of the supercritical region in the neural model of this research is completely different from that of Ref.[50]. We are led to believe that due to the lack of theory that defines the phase transition in biological systems, we cannot certainly determine the type of phase transition. Therefore, this subject remains for future works.

The numerical results shown in Fig. 4.6 to some extent confirm the critical value suggested by Eq. 4.1. Based on this result and explanation provided on Fig. 4.5, three different regimes characterize the order parameter shown in Fig. 4.6. The region *I*, where $0 \leq K \leq K_C$ is called subcritical regime. Region *II* is the critical regime which denotes where the ML function appears with negligible periodicity contamination and $K \approx K_C$. The gray region indicates an overlap between region *I* and region *II*. The vertical arrow indicates the portion of region *II* where the inverse power law, $1/t^{\alpha}$, distinctly emerges. The Region *III* begins almost immediately after the critical value of Eq. 4.1 and is a region significantly influenced by periodicity.

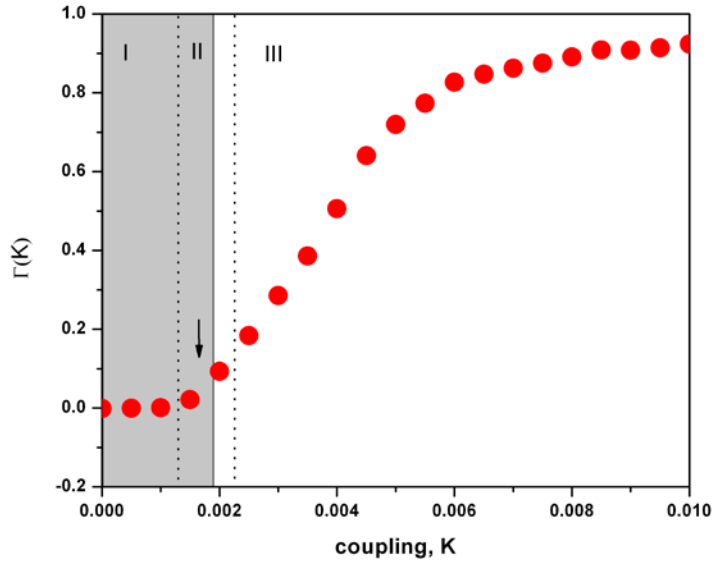

Fig. 4.6. The order parameter $\Gamma(K)$ in terms of K in regular lattice. Three regions or regimes characterize the order in the system: region *I*, subcritical regime where the cooperation is not perceived by neurons, region *II,* critical regime; the region of interest where the temporal complexity is signaled by the ML function and region *III* is the supercritical regime where the system is dominated by periodicity and the ML function breakdown is observed. The gray region indicates an overlap between the two regimes.

To make it easier for readers to understand the effect of periodicity on the ML relaxation, in Fig. 4.7, we have quantified the role of periodicity by means of the property

$$R(K) = E_{\alpha}(-(\lambda T_{MS})^{\alpha}) \tag{4.3}$$

Here, E_{α} is the exact ML function evaluated with the algorithm [51]. In the limiting case of complete periodicity, the survival probability $\Psi(t) = 1$ and $R(K) = 1$. In Fig. 4.7 we see that at $K < K_C = 0.0018$, and $R(K)$ is negligible and undergoes a fast increase when we move beyond K_C.

This would be a convincing indication that criticality has the effect of triggering periodicity, if the critical value was proved to be a genuine criticality parameter. Finding

a value at which the phase transition occurs is a difficult task because at the moment, a theoretical approach to criticality for cooperative models of this kind is not yet available. Thus, we use two other methods to confirm the conjecture on critical value: i) testing of renewal properties ii) The information transfer.

4.4 Testing of Renewal Properties

The criticality indicator that we are using in this research is temporal complexity, and according to the theoretical perspective of Refs.[50,52-53], temporal complexity is characterized by renewal aging. Renewal aging is a special form of aging that requires the following explanation. Aging is a property processes not in equilibrium. Assume that a system is prepared at time $t = 0$ and generates a fluctuation $\zeta(t)$ that is studied by its autocorrelation function $\langle \zeta(t_2)\zeta(t_1) \rangle$. $\langle \dots \rangle$ refers to the Gibbs ensemble average.

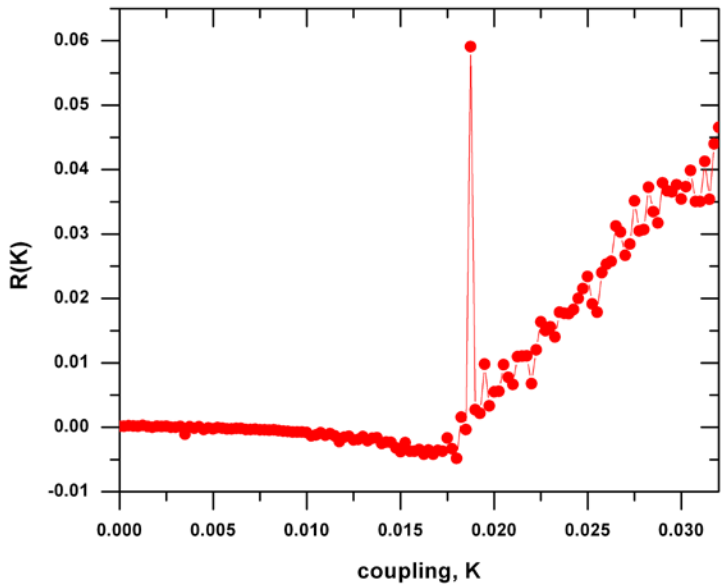

Fig. 4.7. Quantitative measure of periodicity for different values of cooperation parameter. A peak is observed at criticality where it is interpreted as the onset of periodicity.

We observe an infinite number of systems, each generating fluctuations and undergoing an out-of-equilibrium preparation at time $t = 0$. For each system, we calculate the product $\zeta(t_2)\zeta(t_1)$ and the average $\langle\zeta(t_2)\zeta(t_1)\rangle$ over all realizations. For thermodynamical equilibrium systems, the correlation function depends on $|t_2 - t_1|$, corresponding to the stationary condition. This condition is ensured in the case where transition from out of equilibrium to equilibrium occurs with a finite time scale $T_{eq} < \infty$. Hence, if $t_2 > t_1$ and $t_1 \gg T_{eq}$, we have $\langle\zeta(t_2)\zeta(t_1)\rangle = \Phi_\zeta(t_2 - t_1)$. This stationary condition is not fulfilled if $t < T_{eq}$, in which $T_{eq} = \infty$. Hence, the process is a non-stationary process.

This description of the non-stationary process leads to the conventional definition of aging as a process with correlation functions that not only depend on $t_2 - t_1$ but also on t_1. $t_1$is the age of the system. We need to turn the observation of a single time series into the observation process of an infinite number of copies of the same system. This is made possible by the renewal assumption: when an event occurs the system is supposed to have a new time evolution that does not have any memory of the earlier dynamics. The probability of occurrence of new events is exactly the same as if the system were born at the moment of producing that event.

Thus, we generate a number of sequences $\{\tau_i\}$; each of them derived from the same time series. This procedure produces infinitely copies of the same system, which are characterized by the occurrence of an event at the time origin. Using the same perspective, we can describe a time series as an ensemble of age t_a denoted as $\{\tau_{a,i}\}$. This can be extended to all time series; beginning at a time t_a after the first event. This set of sequences can be interpreted as a system of age t_a. Note that this corresponds

to the theoretical prescription in Ref.[54] to apply the Gibbs prescription. The method used here is called the aging experiment, to assess whether or not the process is renewal.

4.4.1 Non-Stationary Correlation Function

The correlation function of age t_a, $\Phi_\zeta(\tau, t_a)$, is defined as

$$\Phi_\zeta(\tau, t_a) \equiv \langle \zeta(t_2)\zeta(t_1) \rangle \tag{4.4}$$

Here, $\tau \equiv t_2 - t_1$ and $t_a = t_1$.

We observe the system's fluctuation at time t_a far from the preparation time. According to a coin tossing prescription, we create a dichotomous signal by assigning either the value $\zeta = +1$, and $\zeta = -1$, to the time regions between two consecutive firings. The correlation function of age t_a is determined by means of a moving window of size t_a, with the left end located at the moment of a firing. We evaluate the time distance between the right end of the window and the first firing after that. The corresponding waiting time distribution is normalized and its survival probability is the non-stationary correlation function of Eq. 4.4. It is expected that the aged survival probability display slower de-correlation upon increasing the age. The procedure is shown in Fig. 4.8. Apparently, if $t_a = 0$, the correlation function coincides with the normal survival probability of Eq. 2.2.

The sequence of time distances can be shuffled and the comparison between the shuffled and not shuffled aged survival probability allows us to assess if the process is renewal or not. If the shuffled and non-shuffled coincide, we conclude that the process is non-Poisson and renewal while if they don't coincide, the process is not renewal.

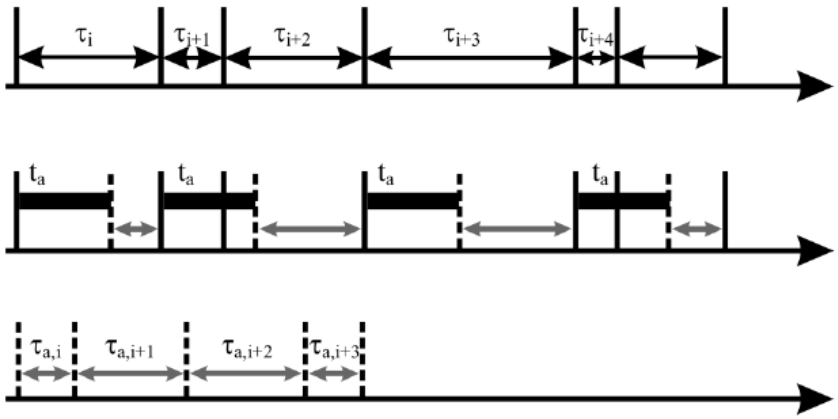

Fig. 4.8. The aging experiment. The top Panel illustrates the original sequence of waiting times$\{\tau_i\}$.Horizontal bars on the middle Panel represent aging time t_a. Gray arrows on the bottom Panel represent obtained aged times $\{\tau_{a,i}\}$ [50].

With this procedure, we obtain the result of Fig. 4.9. In Panel a of the figure, the procedure is done on the system at criticality, $K = 0.0018$ and in Panel b the system at supercritical regime which is dominated by periodicity, $K = 0.0032$. We see that for the critical value, the process is totally renewal and according to our prediction the value of criticality according to Eq. 4.1 is confirmed, while for the system at supercritical regime, the process is not renewal in the long-time regime.

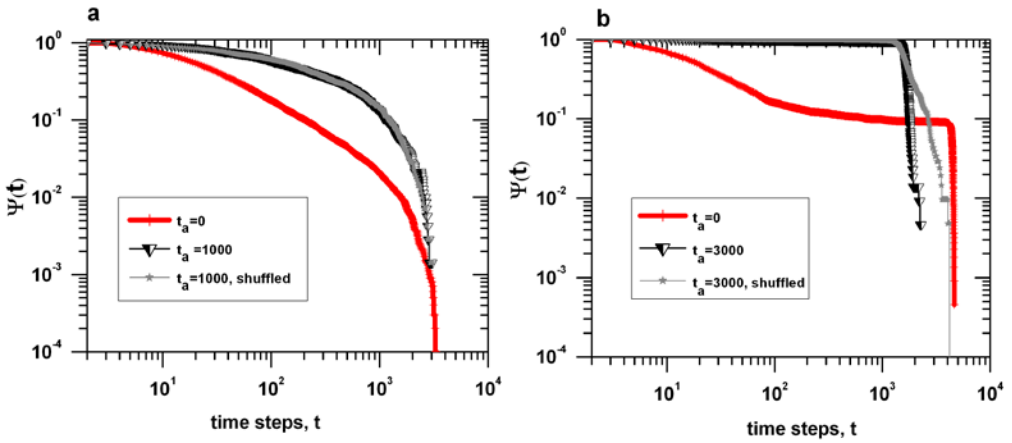

Fig. 4.9. The aging experiment on the system for $K = 0.0018$ (a), and for $K = 0.0032$ (b). The choice of age depends on the time that system starts truncation. In the former case the process is totally renewal, while in the latter the long time is not renewal due to periodicity.

4.4.2 Aging Intensity

Renewal aging is a manifestation of deviation from the condition of ordinary thermodynamical equilibrium and can be used to measure the departure from the Poisson condition. Cooperation makes the neural system violate the Poisson condition. Therefore, aging can be used as an indicator of the transition from the non-cooperative to the cooperative behavior. We evaluate the aging intensity by using

$$\delta(t_a) = \int_0^t |\Psi_a(t) - \Psi(t)|\, dt \tag{4.5}$$

Here, $\Psi_a(t)$ denotes the survival probability of age t_a. Fig. 4.10. shows that $K_c = 0.0018$ belongs to the region of cooperation where the aging intensity increases abruptly.

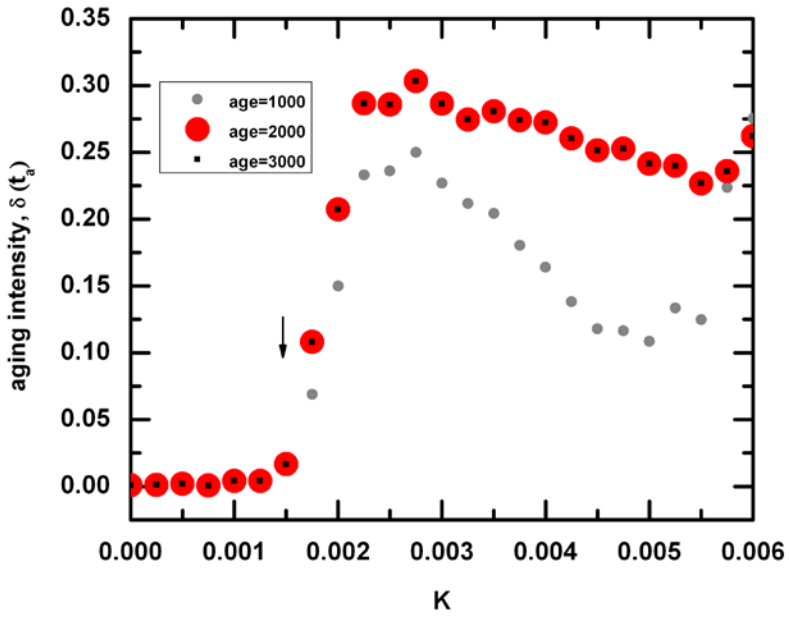

Fig. 4.10. Aging intensity for different values of cooperation parameters and different ages of the system. The arrow indicates the value of K expected to correspond to the genuine criticality of the process.

It is important to note that the maximal amount of aging intensity is observed at values of K significantly larger than $K_c = 0.0018$, thereby suggesting that criticality may hold

true for larger values of K. We must stress that in this kind of experiment, the aging intensity is evaluated with no distinction between renewal and non-renewal aging, and that for values of K larger than K_c, periodicity may break the renewal condition.

Based on the results of this section, we claim that the critical point of Eq. 4.1 is confirmed to some extent. If this is proved by means of information transfer in the next section, we are led to conclude that temporal complexity is a proper measure of criticality.

4.5 Information Transfer at Criticality

There are many simulations in the literature claiming that at criticality, the brain shows maximal functionality through information transfer [11-13], information storage [14-15] and dynamical range [10]. Hence, if there is a point at which correlation and mutual information between two networks is maximal, that point would be criticality. We use this measure to confirm the criticality found by temporal complexity.

Thus, we study two identical networks: network S and network P with the same initial conditions. We perturb network S with network P and monitor the transmission of information from network P to network S. The coupling of S with P is as follows; We select randomly a subset ΔS of the neurons of the network S, moreprecisely 3% of the neurons of S and a subset ΔP namely 3% of neurons of system P. Each neuron of the subset ΔS iscoupled with a neuron of the subset ΔP and is forced to adopt its trajectory, $x(t)$. The spiking pattern of network S before and after perturbation and spiking pattern of network P are illustrated in Fig. 4.11. As is seen from this figure, after a short time, two systems start synchronizing signaled by overlapping spiking pattern.

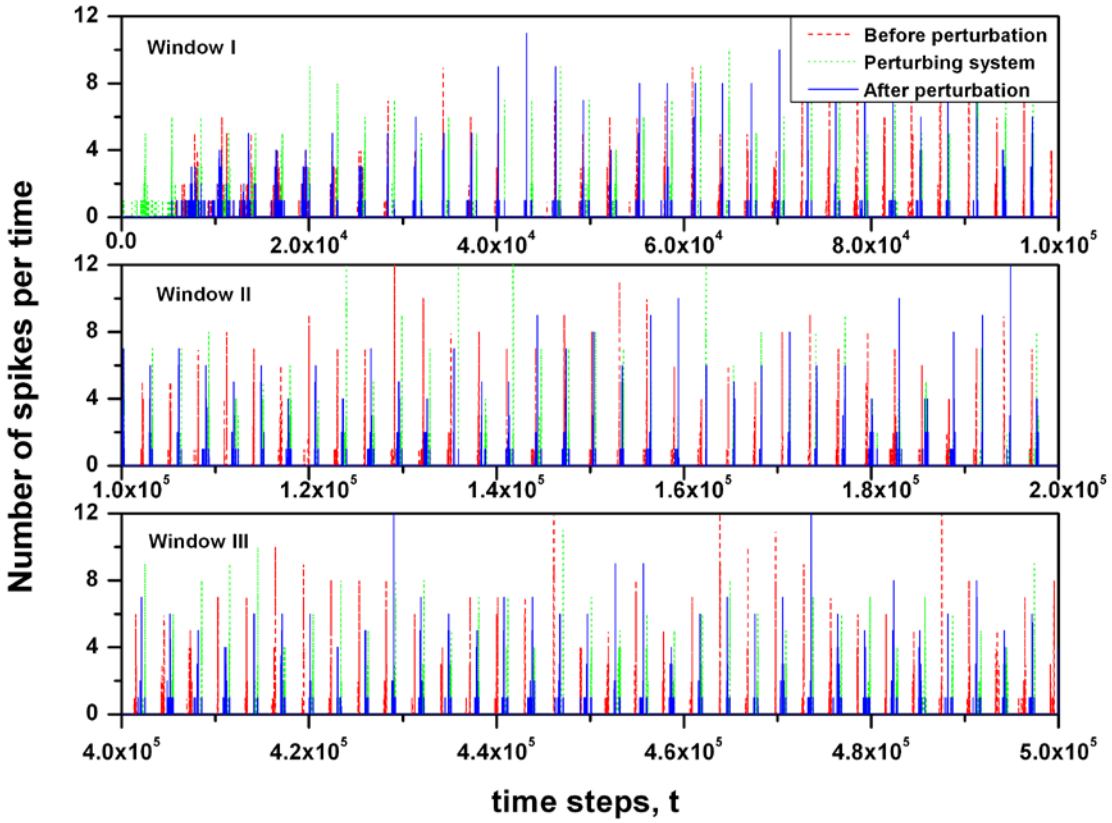

Fig. 4.11. Spiking pattern of Network S before and after perturbation and spiking pattern of Network P. Only 3% of nodes are perturbed. In window I, it takes a while for system S to respond to system P. Thereafter, the two networks are almost synchronizing. Two other windows are showing a better resolution of the spikes in time.

We study the correlation of the network S with the network P by means of the correlation function [55]

$$C(X,Y) = \frac{\sum_{i=1}^{N}(X_i - \bar{X})(Y_i - \bar{Y})}{\sqrt{\sum_{i=1}^{N}(X_i - \bar{X})^2 (Y_i - \bar{Y})^2}} \tag{4.6}$$

The calculation is done at a given time of the order of 10^5. Increasing the observation time leads to the saturation of correlation. The symbols X_i and Y_i denote the membrane potentials of the neurons of the network S and network P, respectively. The

sum runs from $i = 1$ to $i = N$, where N is the total number of neurons of each network, and the result is virtually independent of the order adopted to identify the neurons. The symbols $\bar{X}$ and $\bar{Y}$ denote the mean trajectory of networks S and P, respectively. To study the transmission of information from P to S, the adoption of mutual information seems to be appropriate. Thus, we also study the mutual information that reads as [56]

$$MI(X,Y) = \sum_{X_i \epsilon S} \sum_{Y_i \epsilon P} P(X_i, Y_i)\, lo\, g \left(\frac{P(X_i, Y_i)}{P(X_i) P(Y_i)} \right) \tag{4.7}$$

Here, $P(X_i, Y_i)$ is the joint probability of finding $X_i = x$ and $Y_i = y$ at the same time. The numerical results are shown in Fig. 4.12. We see from the figure that correlation and mutual information reach their maximal value at $K_C = 0.0018$, thereby leading us to conclude that this is the critical value of the control parameter K. We must point out that the crucial result of Fig. 4.12 depends on the adoption of the following initial state: when network S is coupled to network P, which is already in the cooperative regime corresponding to K, all the neurons of network S are in the resting state.

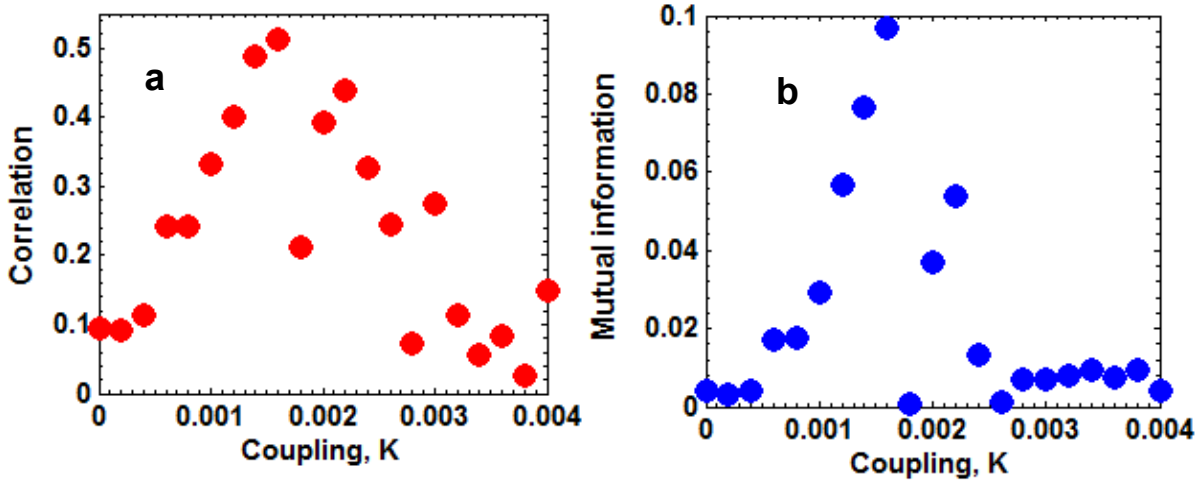

Fig. 4.12. Transmission of information from network P to network S. Correlation and mutual information are evaluated using Eq. 4.5 and Eq. 4.6, respectively. In both cases, the maximum is observed at criticality supporting the value suggested by Eq. 4.1.

If the neurons of S are randomly distributed, the results become statistically less reliable, and show a shift of the maximum towards $K = 0.0032$. The lack of accuracy prevents us from discussing this condition more. We limit ourselves to noticing that the choice of the initial condition generating Fig. 4.12 may be appropriate to studying the transmission of information. Hence, the condition with all the neurons in the resting state implies that the system is able to adapt itself to the directions of system P.

4.6 Self-Organized Criticality

Self-organized criticality (SOC) is a property of dynamical systems that moves the system toward a self-organized mode at criticality [6]. This behavior is characterized by a scale-free spatial and /or temporal distribution at criticality without the need to tune control parameters to precise values. [6]

The paradigm used to define the SOC is the sandpile model. In this model, sand grains are added to a pile. When additional grains are added randomly, inevitably, the slope's local steepness surpasses a certain critical threshold, thus causing a local failure of structural stability. The excess of grains will cascade into neighboring areas of the pile, causing their failures as well. This will cause an avalanche, changing the unstable state of the sand pile into a new, stable state. Here, the important process is propagation of the local random event quickly through the entire system, thus establishing long-range correlations within the system.

In 2003, Plenz and Beggs observed for the first time that the distribution of avalanche size and duration display scale-free distribution [8]. They used a living neural

[6]This property was introduced by Per. Bak, Chao Tang and Kurt Wiesenfeld ("BTW") in a paper published in 1987 in Physical Review Letters [6].

network on the Microelectrodes array and recorded Local Field Potentials (LFP).[7] Their experimental results showed that at criticality, the avalanche size distribution follows an inverse power law of 1.5, and avalanche time duration follows an inverse power law of 2 as theorized by Zapperi *et.al*. [57] using the branching process. In a portion of their experiment, they added bicuculline to the neural network to make it totally excitatory. Despite their expectation that the systems would display smaller scaling of power law index and bigger avalanches, they observed that the scale-free distribution was destroyed. Based on their results, they concluded that the brain as a complex system works near criticality with the hallmark of 1.5 for avalanche size distribution. After they published their results, many other papers were published to confirm those results, while few contradicted them.

Hence, it is interesting to know if the neural networks of this research follow this widely shared conviction. To accomplish this, we use the same numerical treatment as that of Ref.[8] to evaluate avalanches. We consider a time distance of length $\Delta t = 5$ during which two spikes lie into one avalanche. The results not shown here indicate that the choice of Δt changes the results. However, we observed that upon an increment of K, power law indexes of the avalanche probability densities would not change with further increasing of the time step. Therefore, for our numerical calculations we rest on the assumption that $\Delta t = 5$. The results on avalanche size distribution and time duration are shown in Fig. 4.13.

[7] Local Field Potential is a type of electrophysiological signal dominated by the electrical currents of the nearby synaptic activity within a volume of a tissue.

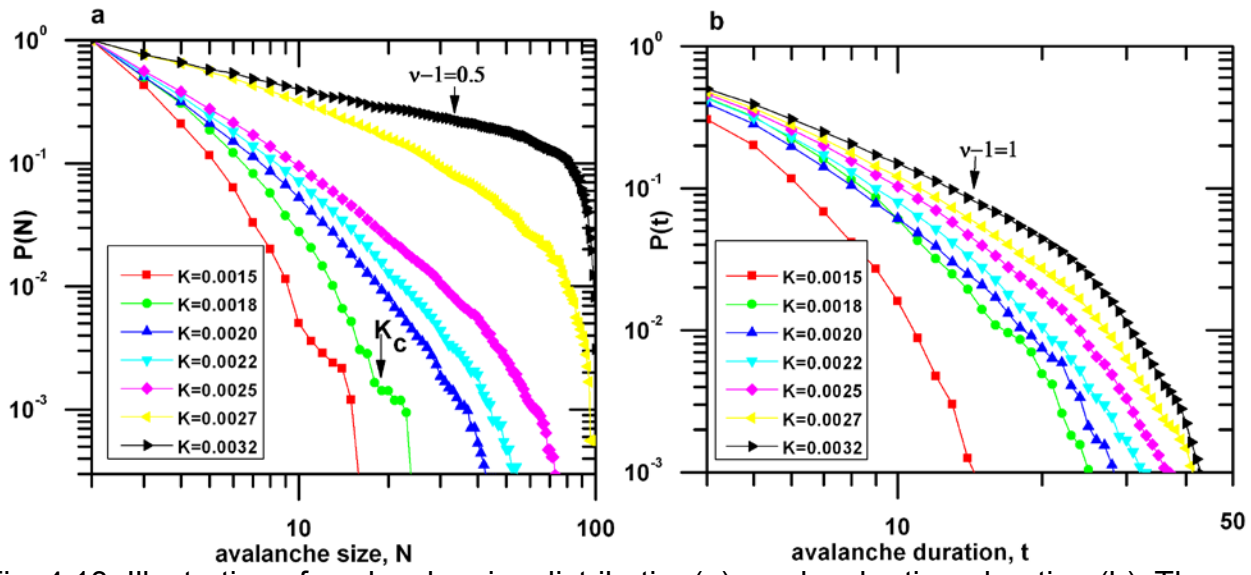

Fig. 4.13. Illustration of avalanche size distribution(a), avalanche time duration (b). The arrow on black curve of each Panel indicates the crucial inverse power law index of each distribution. The red curve in both panels corresponds to the criticality that does not coincide with the black curve.

We see that the crucial power index of avalanche size distribution, $\nu = 1.5$, and the crucial index of avalanche time duration, $\nu = 2$, appears at $K = 0.0032$. This value of cooperation parameter is much larger than the value of criticality predicted by Eq. 4.1. On the basis of these results, we are led to conclude that the neural system under study does not fit the SOC predictions that the power law behavior of avalanche size and time duration distributions are a manifestation of criticality.

This contradiction is due to the fact that there is no theory connecting the criticality and inverse power law index and also that SOC in vivo requires sub sampling while SOC theories assume full sampling [58]. It is important to point out that the existence of power law does not prove that the system is at criticality, since also non-critical systems may produce power laws [59-60].

However, we found the results of Ref.[23], very similar to our finding on regular lattice. Their close examination of the avalanche scales—using rigorous statistical

analysis, from multi-electrode ensemble recording in cat, monkey, and human cerebral cortices, during both wakefulness and sleep—did not confirm power-law scaling of neural avalanches of Ref.[8]. These results apparently contradict the hypothesis that the brain works at criticality, if the inverse power law of the avalanche size distribution is assumed to be a fair criticality indicator.

Therefore, we are led to conclude that in regular lattice under study, these avalanches are rather a manifestation of supercriticality and correspond to the epileptic condition. The healthy brain is signaled by temporal complexity defined by the ML function.

CHAPTER 5

COOPERATION IN NEURAL NETWORK: BRIDGING COMPLEXITY AND PERIODICITY

Inverse power law distributions are generally interpreted as a manifestation of complexity, and waiting time distributions with power index $\mu < 2$ reflect the occurrence of ergodicity-breaking renewal events. In this chapter, we show how to combine these properties with the apparently foreign clocklike nature of biological processes. Increasing the density of neuron firings reduces the influence of periodicity, thus creating a cooperation-induced renewal condition that is distinctly non-Poissonian.

5.1 Temporal Complexity

As pointed out in the previous chapter, it is necessary to activate the noise $\xi(t)$ [61] to generate temporal complexity. Temporal complexity is compatible with the quasiperiodicity of the single-neuron dynamics. If noise intensity is conveniently small, the time spent by one neuron to move from rest to the threshold potential remains close to T_{MS} of Eq. 3.3. Although this condition is ensured by setting $\sigma < \sqrt{\gamma}$, making the mean time distance between two consecutive firings of the same neuron very close to T_{MS}, in the absence of cooperation, periodicity is totally lost. This is a consequence of the noise action. For very low values of K, the dynamics of the whole system are determined by the uncorrelated motion of many units, with the time scale T_{MS}. Due to the lack of correlation, the time distance between two consecutive firings of a set of N neurons is given by Eq. 3.17 with $\langle \tau \rangle = T_{MS}$. As a consequence, the survival probability $\Psi(t)$ namely, the probability that no firing occurs up to the time t from an earlier firing, is

given by Eq. 3.18 which is the typical form of Poisson dynamics. According to the conviction of Ref.[62] that cooperation generates scale invariance, one would expect as an effect of increasing K a transition from the exponential form of Eq. 3.18 to

$$\Psi_C(t) = \left(\frac{T_C}{T_C + t}\right)^{\alpha} \tag{5.1}$$

Where $\alpha \equiv \mu - 1$ with T_{MS} so small as to make Eq. 5.1 virtually equivalent to the inverse power law of Eq. 2.1 over the available time scale (This is Eq. 2.8 that is reiterated for the sake of index reference; C refers to *complexity*). As shown by Fig. 5.1, we find instead that for small values of N, the survival probability is identical to the Mittag-Leffler (ML) function [24,46,63]

$$\Psi(t) = E_{\alpha}[(-\lambda_{\alpha} t)^{\alpha}] \tag{5.2}$$

if we neglect the periodicity-induced long-time truncation.

As explained by the authors of Ref.[24], the ML function plays an important role in the field of complexity because it settles the controversy between the advocates of stretched exponential functions and the advocates of inverse power law as important signatures of complexity. In fact, in the time region $t < 1/\lambda_{\alpha}$ the ML survival probability is described by the stretched exponential function

$$\Psi(t) \propto exp[(-\lambda_{\alpha} t)^{\alpha}] \tag{5.3}$$

and in the large time region $t > 1/\lambda_{\alpha}$ by

$$\Psi(t) \propto \frac{1}{t^{\alpha}} \tag{5.4}$$

The cooperation-induced emergence of the ML function matches the expectation that cooperation generates scale invariance. In fact, the index α of the stretched exponential function of Eq. 5.3 is identical to the power index α of the inverse power law of Eq. 5.4.

On top of that we show that the ML function of Eq. 5.2 is the visible manifestation of a hidden survival probability with the inverse power law form of Eq. 5.1, which is thought to be a signature of complexity [62].

To prove this important fact, we notice that as an effect of cooperation neurons tend to fire at the same time [43,46], thereby making the distance between two consecutive firings become larger than $1/G$ and the intensity of each firing larger than the intensity of a single firing.

As a consequence of the fact that the neural network has a finite number of units, N, some of these multiple firings cannot be realized, or, let us say, they are not visible. If we increase N while leaving T_{MS} constant, thereby increasing the density of neuron firings, all the cooperation-induced multiple firings are realized and are visible, and they are expected to generate a *complex* survival probability $\Psi_C(t)$. Note that this form of temporal complexity yields the ergodicity breaking of Refs.[64-65] when $\alpha < 1$. However, for N small, many firings are not realized. Let us denote by P_S the probability that a multiple firing occurs. Decreasing N makes P_S decrease so that $\Psi_C(t)$, as was explained in Chap.2 and shown in Ref.[46], is replaced by the much slower survival probability of Eq. 5.2 with λ_S satisfying Eq. 2.9 which means that with $P_S \to 0$, $\Psi(t)$ does not decay, signaling that no event occurs.

In the ideal case of perfect synchronization studied by Mirollo and Strogatz [35] the system produces a sequence of firings at times nT_{MS}, with $n = 1,2,..$ with intensity equal to N. When $K = 0$, N firings of minimal intensity, with only one neuron firing, are homogeneously distributed in the time region between $(n-1)T_{MS}$ and nT_{MS}. For intermediate values of K the density of firings in these time intervals decreases, and if

one of these time intervals is empty, with firings of intensity N at both extremes, it will contribute a peak of the waiting time distribution $\psi(t)$ at $t \approx T_{MS}$. The intensity of this peak is proportional to the number of empty time intervals of length T_{MS} .

Actually, as a consequence of working with $\sigma > 0$, the time length of the largest empty time intervals will be smaller than T_{MS}, but these peaks will still perceive the system's periodicity. If the survival probability $\Psi(t)$ virtually vanishes at $t \ll T_{MS}$, as in the high-density case, generating the survival probability of Eq. 5.1 with $T_C \ll T_{MS}$, the influence of periodicity is not perceived, and the intensity of the truncation peaks should be minimal.

Fig. 5.1 fully supports these theoretical arguments shows that lower density yields a slow and heavy tail the ML survival probability. The fast drop in the long-time region close to T_{MS} is due to the high sensitivity to periodicity. It is important to notice that the ML function revealed by the numerical analysis of this article exactly matches the ATA results [43]. This is strong evidence that cooperation generates long-range interactions, thereby making the local-interaction network identical to the ATA network, if a larger K is adopted: Cooperation-induced criticality breaks the local nature of the model [66].

The corresponding low-density $(N = 100)$ waiting time distribution Fig. 5.2 shows a large peak at $t \approx T_{MS}$, while the high-density one $(N = 2500)$ shows no sign of truncation peak, in agreement with the earlier theoretical arguments. For illustrative purposes we have also plotted the perfect synchronization case of $K = 0.1$. It is important to stress that the power law regime of the survival probability of the high-density case is too limited to allow us to use a reliable fitting procedure to find a power

index. Line (b) is a guideline obtained by shifting down the fitting line (a) with the power index of α = 0.75.

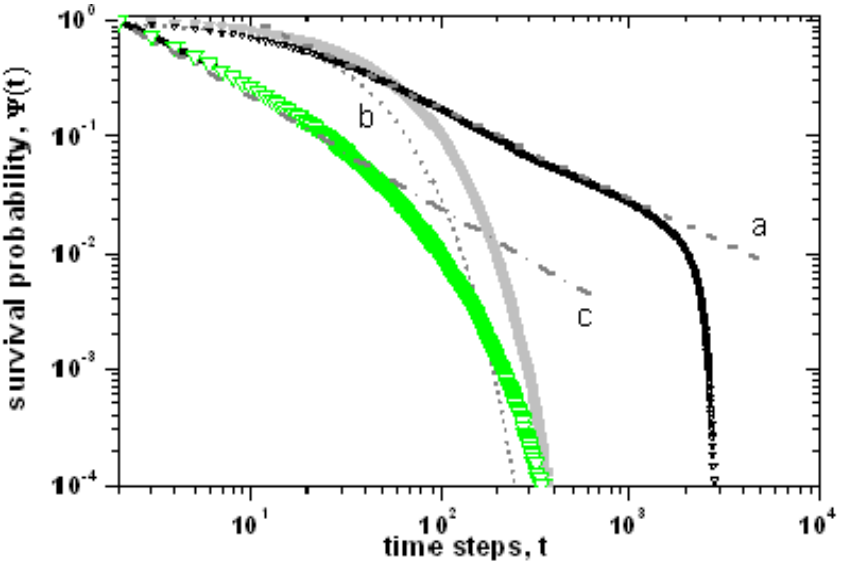

Fig. 5.1. Survival probability of the system with size of $N = 100$ (black curve) for $K = 0.0018$ and $K = 0$ (gray curve), survival probability of the system with size of $N = 2500$ (green curve). The dashed line (a) shows the power law fit, the dotted line (b) shows the exponential fit and the dotted dashed line (c) represents the fitting line parallel to (a).

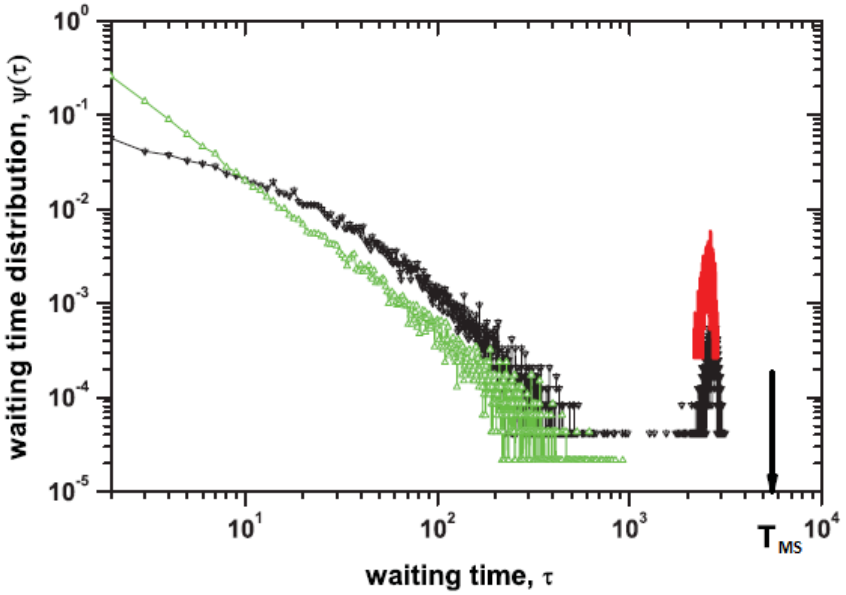

Fig. 5.2. Waiting time distribution for system of finite size (black curve) and the system of infinite size (green curve). The giant peak around the period of the system shows the high resolution of the event with the probability that is not obvious in the high density case.

The reasons of the drop of this power law are not clear. They may be due to random fluctuations influencing the extended transition time regime from. The transition time is not affected by periodicity as clearly proved by the aging experiment (see Fig. 5.2), ensuring that the process is still renewal.

5.2 Cooperation-Induced Renewal Breaking

Let us now address another key issue called the periodicity-induced renewal breaking. The model of this research (namely Eq. 3.1; called integrate-and-fire model) in the absence of stimuli is renewal, since after firing a neuron does not have any memory of the earlier paths. However, under the presence of a harmonic stimulus it may lose its renewal properties [67,68]. The model of this paper, the cooperative LIFM, can be turned into a nonrenewal process without external stimuli, due to the new phenomenon of cooperation induced renewal breaking.

To detect the renewal breaking and to measure its intensity, we adopt the aging experiment explained in section 4.5. It was shown that, if shuffled and unshuffled distributions coincide, the process is renewal. Otherwise the process is non-renewal. Therein, the aging experiment was used to confirm the criticality; we used the age of $t_a = 1000$ for the system at criticality. There is also a range of values that show the renewal property even a little above the criticality. It was also shown in Fig. 4.7 that in the region *II*, the system is contaminated by periodicity.

Hence, in order to show the cooperation-induced renewal breaking, we focus on the value that falls in where is the region that the system is contaminated by periodicity with $K_C > K = 0.002$. Using the aging experiment, we gain the central results of Fig. 5.3.

The age is chosen to be $t_a = 3000$ since the system starts truncation around this time for the low intensity, $N = 100$. We see that the shuffled and the original sequence undergo the same aging effect in the time region $t < T_{MS}$, whereas in the remaining wide time region, the aging of the shuffled sequence departs significantly from that of the original sequence. This is a clear effect of renewal-breaking periodicity.

The events of the short time region are renewable and unpredictable, whereas in the latter time region they may be predictable. Of course, when K is very large, as when it generates the perfect synchronization, the whole process becomes perfectly predictable. Now, we shift to the case of high density, $N = 2500$. In this case the system is not sensitive to periodicity. Using the aging experiment, we gain the results shown in *insert* of Fig. 5.3.

As can be seen in this figure, there is aging, and a strong departure from the Poisson condition, while the virtually perfect coincidence between the results of shuffled and unshuffled procedures proves that the process is renewal. In this ideal case of ordinary complexity, the avalanches are totally unpredictable.

These results help shed light on the predictability of events at the time of crisis [67]. It is clear that the predictability would be explained knowing the density of units or events in the system. As was shown, if the system truncates at the time very close to the period of the system, signaling periodicity; it would be easier to imagine the possibility of prediction in the system. However, in the case of large density, the probability distribution of events would not truncate at the system's natural time, but much earlier as to make it very insensitive to the periodicity.

5.3 Neural Avalanches

We note that the results of Fig. 5.1 do not afford any direct information on the quake intensity. To discuss this problem, we study the distribution of avalanche sizes for different values of N. Avalanches are a well-known property of neural networks and as was shown in Chap.4 the neural network of this research generates avalanche distribution with power index of 1.5 for the avalanche size and 2 for the avalanche duration matching the experimental observation of Ref.[8].

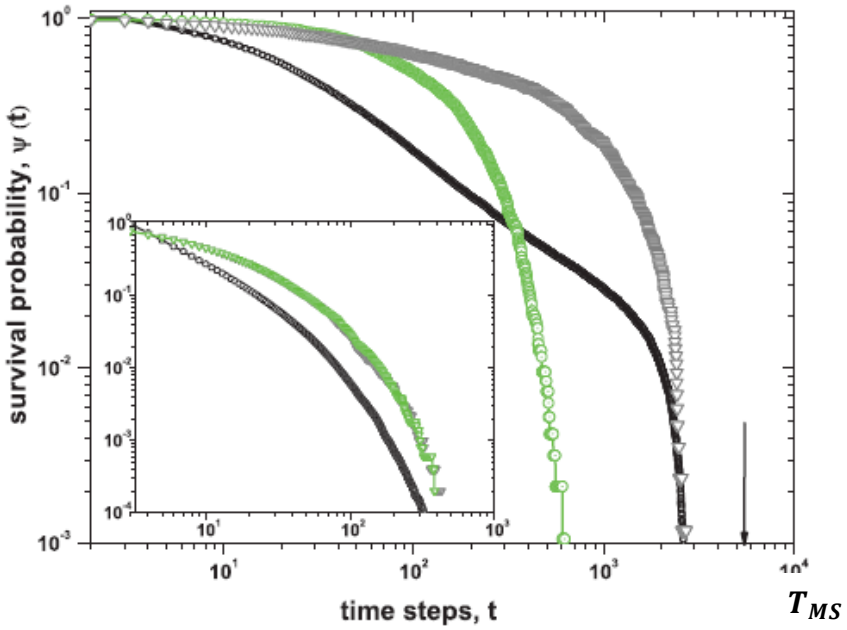

Fig. 5.3. Cooperation-induced renewal breaking of the low intensity case, $N = 100$ and $K = 0.002$. In the short time regime the process is renewable and unpredictable, while in the long time it is non-renewable and predictable. *Insert*: Cooperation-induced renewal breaking of the high intensity case, $N = 2500$ and $K = 0.002$. The coincidence of shuffled and un-shuffled distribution indicates that the process is totally renewable and unpredictable.

Here, we focus on the size distribution. Fig. 5.4 shows that the distribution density of avalanche sizes for a suitably large value of $K = 0.013$ is characterized by a bump, and this bump increases with decreasing N, a property shared also by the model

used by de Arcangelis [70]. The truncation peak corresponds to the ideal synchronization of Mirollo and Strogatz [35], namely, to an avalanche of maximal intensity N. Setting $\sigma = 0$ prevents small avalanches to unfold, a limiting condition of periodicity with no temporal complexity, which according to the inset of Fig. 5.4 extends to a small range of σ values. Gigantic avalanches of size N may coexist with temporal complexity and with the experimental power law distribution of index $\upsilon = 1.5$, and the fraction of avalanches of maximal intensity emerging from a power law background becomes larger with decreasing the neuron density, due to the close connection between sensitivity to avalanches and the heavy tails of $\Psi(t)$.

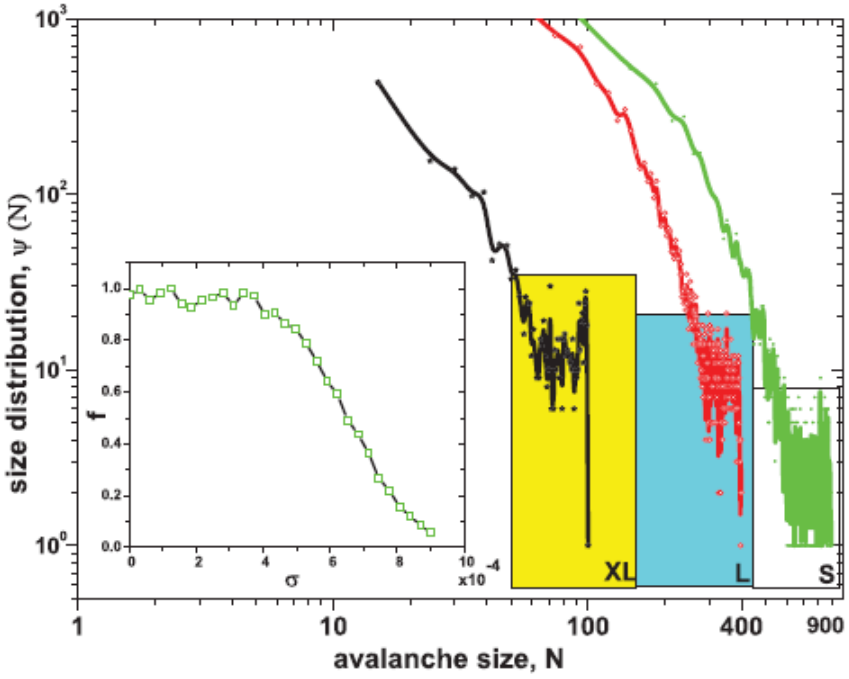

Fig. 5.4. Avalanche size distribution for $N = 100$ (black curve), $N = 400$ (red curve), and $N = 900$ (green curve). In all three cases $\sigma = 0.0001$ and $K = 0.013$. Data are log-binned. *Insert*: Fraction of the number of the avalanches of intensity N to the total number of avalanches, as a function of σ.

5.4 Summary

The results of this chapter shed light into the coexistence of periodicity and complexity. In spite of the fact that each neuron interacts only with four nearest neighbors, suitably large values of K make this model recover the perfect synchronization of Ref.[35]. However, an extended regime exists between the weak-coupling regime, where the units of the system are independent of each other, and the perfect synchronization regime. In this intermediate regime, periodicity and complexity coexist.

This may contribute to the foundation of a theory for the occurrence of Dragon Kings proposed by Sornette, a new phenomenon that is currently the object of a vigorous debate [71-72]. The Dragon Kings are anomalous events emerging from a power law background. This paper establishes a connection between the existence of Dragon Kings and the apparently conflicting coexistence of renewal and nonrenewal properties in the same complex model. Interpreting the Dragon Kings as outliers [72] generates the impression that they are foreign to the cooperation-induced locality breaking from which temporal complexity emerges. We make the conjecture that the peaks emerging at the maximum value of avalanche size distribution N coinciding with the total number of neurons are the Dragon Kings of Refs.[71-72]. If this interpretation is correct, the Dragon Kings would be a manifestation of the same cooperation-induced long-range correlation as that proved to be essential for the function of complex systems [66].

Last but not least, the results obtained here may be general. The adoption of a regular two-dimensional network has been decided as the simplest way to assign to

each neuron the same number of links. On the basis of the results of the recent work of Ref.[73] we make the plausible conjecture that the adoption of different network topologies generates temporal complexity, locality breakdown, and perfect synchronization upon changing the values of K. There may be scale-free networks where all the results of this paper are recovered at lower values of K.

In fact, the work of Ref.[73] shows that the cooperative system generates dynamical links with a scale-free structure that has the important effect of facilitating the transition from the Poisson condition to the criticality-induced long-range correlation regime. However, while the cooperative model used in Ref.[73] is Ising-like, and is renewal for both low and high values of the cooperation parameter [50], by contrast, the model of this research shows a transition from the renewal condition (at the emergence of criticality) to a predictable nonrenewal coherent regime as the cooperation parameter K increases as was shown in Chap.4.

CHAPTER 6

TWO SOURCES OF POWER LAW TRUNCATION

In this chapter, two distinct sources of power law truncation of the ML function are presented. To the best of our knowledge, there is still no map that generates the ML function. However, we use the power law truncation of survival probability generated by Pomeau-Manneville as a map to support the numerical results of this chapter.

6.1 Power Law Truncation

In Chap.4, a fitting procedure was used by applying a Laplace transformation on survival probability. In this procedure, fitting parameters, α and λ, were found numerically. The behavior of survival probability was interpreted as the ML function that shows a stretched exponential at short time regime and inverse power law at long time regime.

The ML function may be generated by calculating cumulative probability on the time series generated by the algorithm [74]

$$\tau = \frac{1}{\lambda} ln\left(\frac{1}{u}\right)\left(\frac{\sin(\alpha\pi)}{\tan(\alpha\pi v)} - \cos(\alpha\pi)\right)^{1/\alpha} \tag{6.1}$$

Where $u, v \in (0,1)$ are independent uniform random numbers, λ is the scale parameter, and τ is a Mittag-Leffler random number. There is also another algorithm that generates the ML function directly for given α and λ [51].

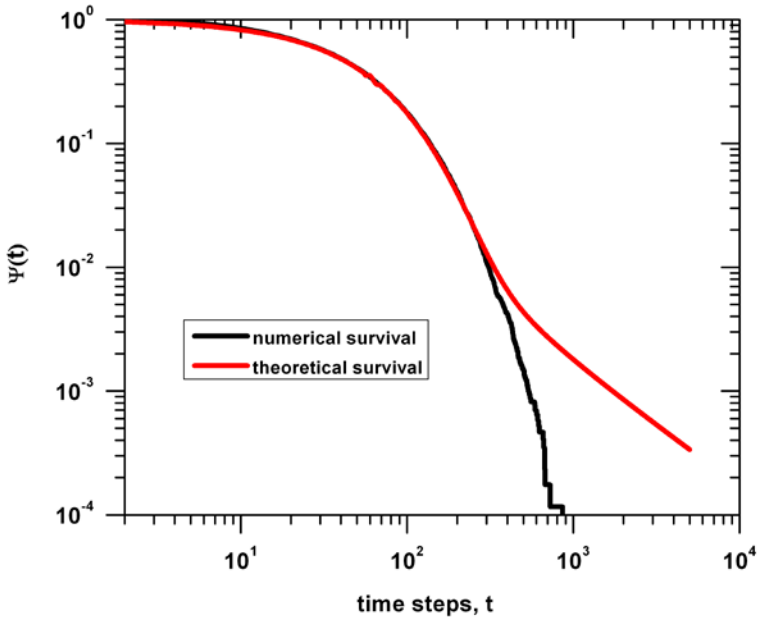

Fig. 6.1. Comparison of the ML function emerging from neural system with theoretical ML function generated by algorithm of [51].

To validate the accuracy of the numerical fitting procedure used in Chap.4, we take the fitting parameters gained from the numerical procedure and run the two algorithms mentioned above. Then, we compare the survival probability of the numerical ML function with theoretical equivalent (Fig. 6.1). We found a clear discrepancy in the tail of the ML function for $\alpha < 1$ where cooperation is large enough to make the process first complex and then periodic (See also Fig. 4.5).

Moreover, we showed that three regimes characterize the order parameter as is shown in Fig. 4.7. In region *I*, the power law index remains around 1; namely $\alpha \approx 1$, and the process is a Poisson process, in region *II*, $\alpha < 1$, although this region is not fully contaminated by periodicity. However, periodicity is fully perceived in region *III*. Hence, based on this classification and also the previous study of Refs.[75-76], we presume that the source of truncation in region *I* and *II* is fluctuations while in region *III*, truncation

is due to periodicity. We refer to these truncation sources as noise- and periodicity-induced tail truncations. In the following sections, we explain in more detail.

6.2 Noise-Induced Tail Truncation

To address the noise-induced trail truncation, it is essential to study the fluctuations effect on the survival probability distribution analytically and numerically. For analytical study, after searching in the literature, we are confident that a map that generates the ML function is not yet found. It would be useful to use the theoretical perspective adopted by our group in an earlier study to investigate the noise-induced tail truncation.

Therefore, an explanation of the method used by the authors of Refs.[75-76] is inevitable. These authors have studied the environmental fluctuations in their model using a perturbation of the Pomeau-Manneville map [74].[8] The focus is only on the long-time limit characterized by the inverse power law property

$$x_{t+1} = T(x_t) = x_t + x_t^{1+\frac{1}{\alpha}}, mod\ 1 \tag{6.2}$$

It is possible to make this discrete-time map compatible with a continuous time description

$$\frac{dx}{dt} = a_0 x(t)^{1+\frac{1}{\alpha}} \tag{6.3}$$

Its solution for a trajectory moving from the initial condition $x_0 = v$ reads as

$$x(t) = \frac{v}{\left(1 - \frac{a_0 v^{1/\alpha} t}{\alpha}\right)^{\alpha}} \tag{6.4}$$

[8] This map also generates a form of complexity signaling a power law.

When the trajectory $x(t)$ reaches the threshold $x = 1$, it resets to its initial condition $x_0 = \upsilon$ as is selected with uniform probability in the interval $0 < \upsilon < 1$. If τ is the time necessary to move from the initial condition $x = \upsilon$ to $x = 1$, using Eq. 6.4, we arrived at

$$\tau = \frac{\alpha}{a_0}\left(\frac{1}{\upsilon^{1/\alpha}} - 1\right) \tag{6.5}$$

Similar to the algorithm of Eq. 6.1, this equation generates a time series. This algorithm allows us to address the noise-induced tail truncation. Since a map of the same kind as that of Eq. 6.2 — a map that generates the ML function —is not yet known, the comparison of Eq. 6.5 with Eq. 6.1 suggests a plausible way to understand cooperation-induced processes. In the limiting case of $v \to 0$, both prescriptions yield

$$\tau \propto T(u)\left(\frac{1}{v}\right)^{1/\alpha} \tag{6.6}$$

With $T(u) = \alpha/\alpha_0$ and $T(u) = (1/\lambda)\ ln$ in the case of Eq. 6.4 and Eq. 5.1 respectively.

The Pomeau-Manneville map seems to be appropriate for the inverse power law appearing at large times while for the ML complexity, as suggested by Eq. 6.1, we should use a two-dimensional map that is not yet known. However, to account for the noise-induced power law truncation, we have to apply to this still unknown two-dimensional map the same arguments as those adopted by authors of Refs.[75,76] on the Pomeau-Manneville map.

We assume that, at criticality, a system with a finite number of units obeys the modified Pomeau-Manneville map

$$t_{l+1} = x_t + x_t^{1+\frac{1}{\alpha}} + f_t,\ \ mod\ 1 \tag{6.7}$$

Here, f_t is a random noise of intensity D. The authors of Ref.[74] prove that an extremely small intensity $D \propto 10^{-13}$ may produce a truncation at $\propto 10^4$. The power law

truncation is due to the deterministic dynamics for v very close to zero. The power law may be extremely slow and even slower than the diffusion process generated by the random fluctuation f_t. [9]

In practice, this is equivalent to assuming that the initial condition with $v < \epsilon \ll 1$ is not allowed and that the effective initial condition is ϵ. The algorithm of Ref.[75] suggests that the ML function may derive from the deterministic prescription of a two-dimensional map. Thus, in this case, the noise-induced tail truncation depends on the fact that entering regions $v < \epsilon_v < 1$ and $u < \epsilon_u < 1$ for initial conditions are not allowed. The quantities ϵ_v and ϵ_v are proportional to the noise intensity, and for simplicity, we refer to them as noise strengths.

We ran the neural model of this research for $K = 0.001$. According to Fig. 4.2, this value of the cooperation strength corresponds to the region where the power law tail is not yet visible and the survival probability is still a stretched exponential function. The Laplace fitting procedure was executed to determine α and λ. Using the noise strength $\epsilon_v = \epsilon_u = 0.03$, we ran the algorithm of Ref.[74]. The choice of the noise intensity is based on numerical observations. After assessing the noise intensity to evaluate the tail truncation at $K = 0.001$, we study the condition $K = 0.0018$. This value of cooperation parameter corresponds to criticality according to Eq. 4.1. Repeating the same procedure on $K = 0.0018$, we see that the power law tail becomes visible, in a good agreement with the numerical results. This is because if the power index is reduced, a fluctuation with the same intensity generates a truncation at larger time regimes, according to Eq. 6.6.

[9] Diffusion processes are continuous-time, continuous state-space processes and their sample paths are everywhere continuous but nowhere differentiable.

The interpretation of these results is as follows: at $K = 0.001$ the system begins its transition to the cooperation regime with $\alpha = 0.95$. The fluctuations make the ML tail invisible. Upon increasing the cooperation parameter from $K = 0.001$ to $K = 0.0018$, the ML tail becomes visible, as is seen from Fig. 6.2. The internal noise is not strong enough to annihilate the ML power tail. This source of truncation ought not to be confused with the periodicity-induced truncation, which is signaled by the vertical arrows of both Panels, corresponding to the prediction of Eq. 3.3. The noise-induced tail truncation occurs earlier than the periodicity-induced tail truncation with increment of coupling strength, K.

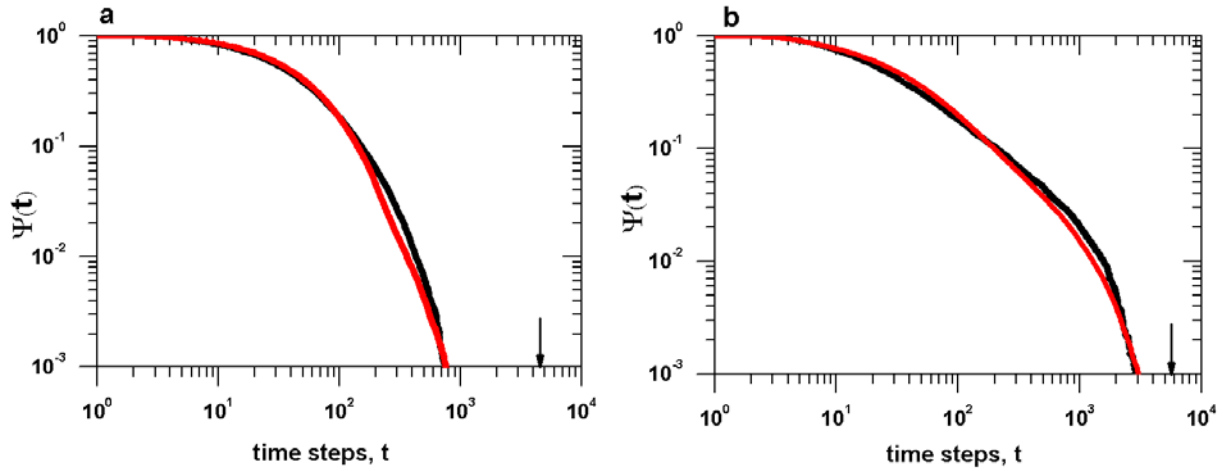

Fig. 6.2. Noise-induced tail truncation. $K = 0.001$ (a), $K = 0.0018$ (b). In both cases, the process is affected by fluctuations.

6.3 Periodicity-Induced Tail Truncation

As was explained in Chap.3, the model of this manuscript is a modified version of the Mirollo-Strogatz model in which all neurons fire at the same time. In their study, Mirollo and Strogatz used an ATA network, while here we studied regular lattice showing the same properties at those of ATA [43], with tuning the control parameter as

the result of network topology. As was discussed in Chap.4, the increment of cooperation parameter in the system, leads to temporal complexity. At temporal complexity, system acts as an ATA network; namely, all neurons get connected, and we are led to conclude that the cooperation results in locality breakdown.

In fact, criticality is the onset of the locality breakdown that becomes more evident when the coupling is larger. If the cooperation is large enough, it puts the system in the supercritical regime denoted as region *III,* where the system reaches the perfect synchronization.

As is seen from Fig. 6.3, the truncation time of the survival probability follows Eq. 3.3—herein $T_{MS} \approx 5300$— for a value of K larger than K_C and higher. The value of cooperation is large enough to make the system fully cooperative. Neurons do not fire up to $T_{MS} \approx 5300$ and finally they all fire at the same time, interpreted as the perfect synchronization. This explanation supports the claim that region *III* of Fig. 4.7 is dominated by periodicity. It is not yet clear what kind of function may define the behavior of survival probability distributions in the periodic regime. Future theoretical study on this process may help shed light on this ambiguity.

Overall, based on the explanations given, we confirmed the division of system dynamics into three categories: subcritical, critical, and supercritical. In the first two regimes, the tail truncation, occurs as the result of fluctuations and is called noise-induced tail truncation, while in the supercritical regime, the system falls into periodicity and its tail truncation is called periodicity-induced tail truncation. An advantage of this system classification is the predictability of events. When the system is affected by a periodic behavior, it is easy to predict the occurrence of events in the future. However,

event forecasting in the fluctuating regimes, as of region *I* and *II* of this model, is unlikely, as was shown by means of the aging experiment in Chap.4

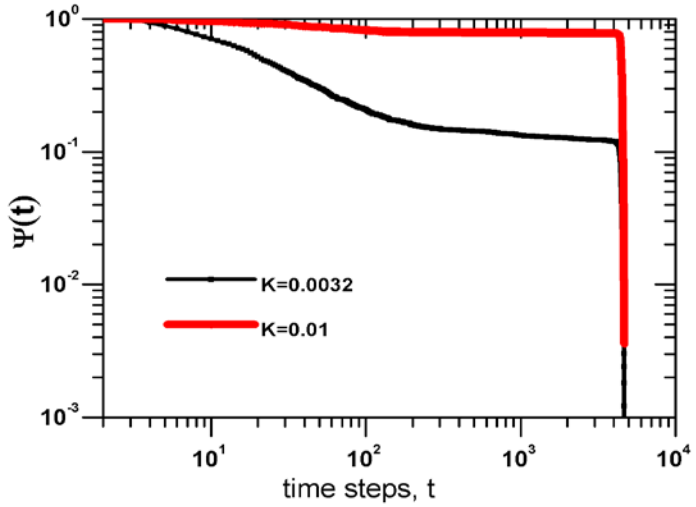

Fig. 6.3. Periodicity-induced tail truncation. Two curves lay into the region dominated by periodicity. $K = 0.0032$ is where system signals avalanche distribution in size of 1.5 confirming our conclusion in Chap.4 on the epileptic behavior of the neural network in that region.

CHAPTER 7

COOPERATION-INDUCED TOPOLOGICAL COMPLEXITY

In this chapter, network organizational dynamics is discussed. We focus our attention on the criticality where the information transfer is maximal, and the network has the highest efficiency. Dynamical observation of the network topology shows that degree distribution follows a power law distribution. It is proved that the newly generated topology is more efficient than an ad-hoc network.

7.1 Network Topological Evolution

The effort to find a rigorous measure of network efficiency is one of the main problems of network science [78]. Network vulnerability may not be addressed without a measure of global efficiency. Network efficiency was originally studied in connection with topological structure [78]. Recently, researchers have discussed the connection between synchronization and topology [79].

It was shown that criticality is where the system shows long-range correlation and synchronization. This effect makes the system equivalent to a fully cooperative system regardless of the resting network that it starts with. [10] Hence, the network properties have a close connection with topological structures that emerge at each level of evolution.

On the hand, it was discussed in Chap.4 that criticality is where the system has maximal functionality such as information transfer due to long-range correlation. We also found a critical point that does not display the crucial power law index of 1.5 for

[10] Resting network is the regular lattice prior to the activation of cooperation. When the network evolves in time, it shows structural properties different from the network at rest.

avalanche size distribution; contradicting the widely shared conviction of criticality and SOC hallmark. Therefore, studying the organizational properties of the neural network may confirm the critical vale found in this research.

Herein, we study the connection between network topology and cooperation parameter. Two different networks are introduced: a resting and a dynamic network; the former is the network that units are at rest; namely in the absence of cooperation and the latter is the network generated by the self-organization of the units located on the structure of the resting network. We argue that these results establish a connection between criticality and the famous Donald Hebb's Neurophysiological postulate [80].

7.2 Cooperation-Induced Network Topology

To study the network topology, we consider the neural dynamics of the present study at criticality according to Eq. 4.1 ($K = 0.0018$). After initial 10^5 time steps, we record lattice configuration over 10^5 time step windows, registering the dynamics of each node $\{x_i(t)\}$ over that time interval. In the next step we evaluate the linear correlation coefficient between the i-th and the j-th node [81]

$$C(i,j) = \frac{\langle x_i(t)x_j(t)\rangle - \langle x_i(t)\rangle\langle x_j(t)\rangle}{\sqrt{\langle x_i^2(t)\rangle - \langle x_i(t)\rangle^2}\sqrt{\langle x_j^2(t)\rangle - \langle x_j(t)\rangle^2}} \tag{7.1}$$

Where $\langle \dots \rangle$ denotes the time average. If the correlation intensity between nodes i and j of the square lattice is larger than threshold value $\Theta = 0.78$, we consider them connected by a link in the dynamically induced topology.

Herein, there are two questions that a reader might ask. i) why we consider the network at criticality and ii) how to define the threshold since newly created topology

depends on selected value of the threshold applied to the set of obtained correlation coefficients.

Regarding to the first question, we know that in the subcritical regime, randomness dominates the cooperation between units and correlation between nodes is almost zero. In the supercritical regime also the periodicity dominates the cooperative behavior while the correlation between units vanishes. However, in the critical regime, the coupling between units is just enough to balance the stochasticity. This condition leads to dynamical coupling between units that are not directly connected and results in wider distribution of values of $C\ (i,j)$ than in two previous cases.

The next question to be addressed is the value of threshold chosen as $\Theta = 0.75$. Considering the network at criticality, adoption of a low threshold would result into the highly correlated nodes and make all nodes connected to each other. As the threshold Θ increases, less pairs would be included in the newly created topology. The increase of threshold leads to the destruction of a giant cluster of links. Thus no new structure can be identified. Close to the selected threshold, the transition between the fully connected structure obtained for low threshold and its destruction into separate modules is more subtle. Fig. 7.2 depicts this explanation visually. The clustering coefficient is calculated using [82]

$$\bar{C} = \frac{1}{N}\sum_{i=1}^{N} C_i \tag{7.2}$$

Where

$$C_i = \frac{3 \times number\ of\ triangles}{Number\ of\ triple\ vertices} \tag{7.3}$$

and N is the total number of units.

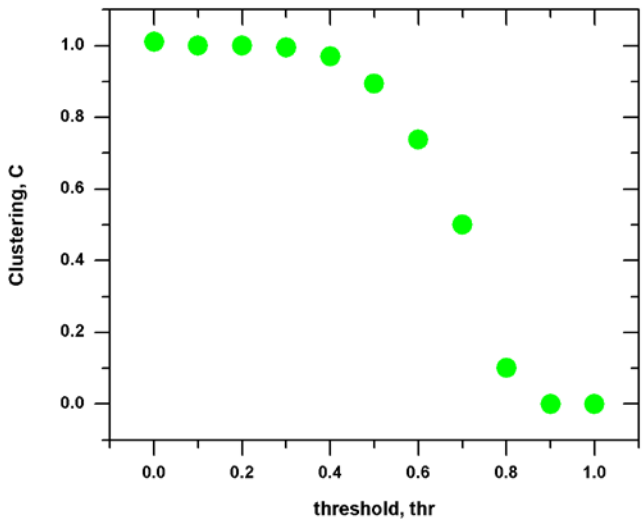

Fig. 7.1. Clustering in the network decreases with increasing threshold. The value suggested by the figure is around 0.78 as is used to study the network evolution.

After choosing the threshold and the value of cooperation parameter, we assess the correlation coefficient. In more detail; after taking time windows of 10^5, the correlation between all pairs $\{x_i, x_j\}$ is calculated which results in a matrix of values between 0 and 1 denoted as weight of connection between nodes w_{ij}. If the correlation between two nodes is high; it implies that they have consistently contributed in firing of each other through links that at criticality would be independent of their Euclidean distance.

After the threshold, $\Theta = 0.78$, is applied, the connection between two nodes is chosen to be 0 or 1 depending on the weight of connections. The resulting matrix is an adjacency matrix of the whole network. Finally the degree distribution of the links in the network is driven from adjacency matrix. As seen the degree distribution displays a scale-free behavior. This result indicates that the network topology is dynamic and this dynamics is stable with scale-free behavior. Fig. 7.2 illustrates the process visually.

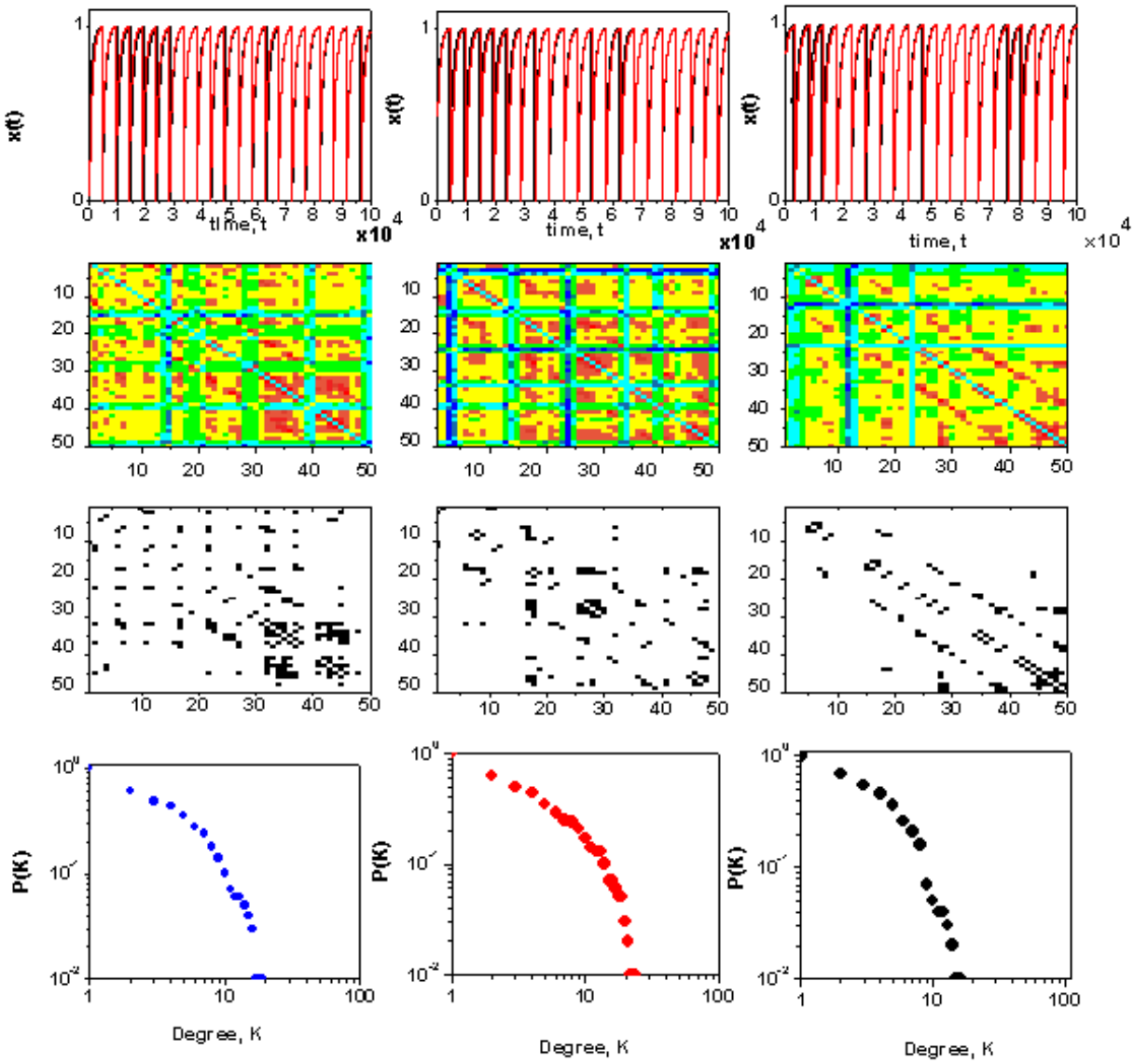

Fig. 7.2. Illustration of the measurement of degree distribution on the network at criticality. Top Panel shows random pairs that the cross correlation is calculated over 10^5 time step windows. This process is repeated for all pairs and is shown as correlation matrix shown in the second Panel. The weight of connections is ranging between zero and 1 shown in different colors. The Third Panel illustrates the matrix of connections after applying the threshold. The bottom Panel shows the degree distribution calculated for each time window.

In other words, we start with a regular lattice whose degree distribution is a Dirac-like distribution. As the result of cooperation, neurons get connected with each other regardless of their predefined connections, and the degree distribution follows

scale-free distribution (See Fig. 7.3). This scaling implies that there are few nodes in the network with large degree; they are linked to many nodes, while there are many nodes in the network with small degree; they don't posses many links.

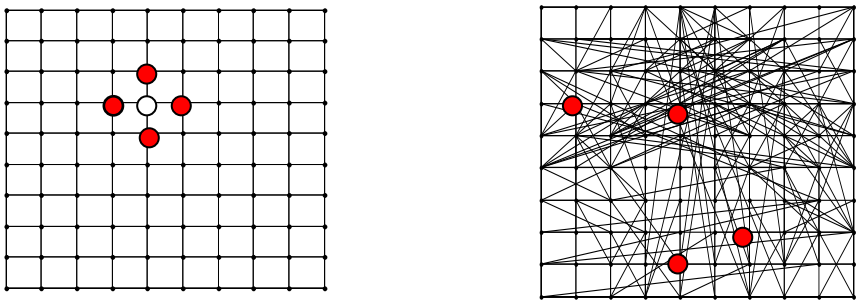

Fig. 7.3. Configuration of the resting network on the right; a node with its four nearest neighbors are marked. On the left dynamical network topology; a node gets connected as the result of cooperation as is marked in the figure.

7.3 Network Efficiency and Learning

In order to study the efficiency of the newly generated network a new measure of network efficiency is used [82]. The authors of Ref.[82] claim that their method is more reliable than the traditional method of network efficiency which reads as

$$L \sim \ln(lnN) \tag{7.4}$$

N is the number of nodes and efficiency is $E = 1/L$ for power law index of $\alpha < 3$ [83]. However this relation applies without no significant dependence on α. While in [82], the method applies to the system of $\alpha \approx 2$ making it a good candidate to be applied on the emergent network at criticality.

According to this method, the Euclidean distance between each pair of correlated nodes is recorded, and the network efficiency as the mean value of this value is defined. In particular

$$P = \frac{1}{N}\sum_{1}^{N}\lambda_i \tag{7.5}$$

Where

$$\lambda_i = \sum_{j=1}^{k_i} d_{ij} \tag{7.3}$$

Here d_{ij} is the Euclidean distance between node i and node j connected to it [83]. P is defined as perception length. It is expected that at criticality, due to the long-rang correlation, the perception length is high; implying to the higher efficiency.

In order to compare the efficiency of the newly generated network, we generate an ad-hoc network with the same α is generated and embedded that in a regular lattice. The perception length of each network is calculated. The results in table 1 show that created network, emerged from a regular lattice is more efficient that an ad-hoc network.

Table 7.1. Comparison between network efficiency of dynamically generated network and ad-hoc network.

	$\boldsymbol{\alpha}$	Perception Length, P
Dynamical Network	1.1	280.8
Ad-hoc Network	1.15	204.4

Donald H. Hebb states that: “let us assume that the persistence or repetition of a reverberatory activity (or "trace") tends to induce lasting cellular changes that add to its stability. When an axon of cell A is near enough to excite a cell B and repeatedly or persistently takes part in firing it, some growth process or metabolic change takes place in one or both cells such that A's efficiency, as one of the cells firing B, is increased.”

We interpret the results of this chapter in the light of this hypothesis. We found that during a finite but long enough time, the regular lattice is transformed into a network whose degree distribution follows the power law distribution of $\alpha \approx 1$. This dynamically generated network is consistently changing and the leadership is passed through the nodes as the result of equivalent nodes. After many organizations, according to Hebb's postulate, recurring dynamical links are turned into resting links. This may also address to the fact that during life, the human brain rewires to make the most efficient scaling. In a study of brain network evolution [84], MRI images of babies from 3 weeks to 2 year-old showed that the temporal and spatial evolution of brain network topology are constantly changing. The brain possesses the scale-free topology immediately after birth. This topology remarkably improves the efficiency in 1 yr olds and becomes more stable in 2 yr olds. This result also reveals that the network organization and development continues towards higher order of cognitive function and intelligence [83].

CHAPTER 8

GENERAL CONCLUSION

In this dissertation, a system of neurons that models some behaviors in the brain such as spontaneous activities, fluctuations, local, and long-range interactions is studied. The neural system of this research is a system of cooperative neurons in a regular lattice; each neuron is connected to its four nearest neighbors. Using the leaky integrate-and–fire model, the network generates a spiking pattern, with neural avalanches in size and duration coinciding with the experimental results both *in vivo* and *in vitro*. Cooperation is defined as the control parameter of the system. Focusing on temporal complexity and fractal index of the system, it is discussed how to define an order parameter. Criticality is assumed to correspond to the emergence of temporal complexity, interpreted as a manifestation of non-Poisson renewal dynamics. It is shown that the system makes a transition from a non-cooperative state to a fully cooperative state where complexity emerges in between.

As a rigorous proof of criticality, the study of information transfer from one network to another show the maximal correlation and mutual information at criticality suggested by temporal complexity. Distribution of neural avalanches in size at criticality does not display power law scaling of 1.5, contradicting the widely shared conviction that has emerged from research on neural networks, while coinciding with the few recent experiments on the real brain.

Moreover, the coexistence of complexity and periodicity as a result of the emergence of ML function was revealed supported by analytical and numerical calculations.

Studying the network evolution, a cooperation-induced topology is found whose degree distribution follows inverse power law scaling. It is discussed that this result may be interpreted as the brain development during life toward highest order of cognitive behavior.

However, there are still issues that remain unanswered. From neurobiological point of view one major problem is the lack of inclusion of inhibitory synapses in the model. Another is the integration of synaptic depolarization and hyperpolarization over the complex morphology of a neuron which here was considered in a single step. From Theoretical point of view, the most pressing problem is assessing the connection between criticality and self-organization hypothesis. A more rigorous theory on definition of temporal complexity and its connection with avalanche size distribution is needed to allow exploration in wider ranges of application, and helps to understand the impact of each parameter on the observed behavior of the system. Also considering inhibition in the neural system would make it more realistic. Despite those obstacles, presented work creates a promising foundation for this future research on the brain.

APPENDIX A

SUBORDINATION APPROACH ON SURVIVAL PROBABILITY

Let us denote by $\Psi(t)$ the survival probability corresponding to a given P_S. When $P_S = 1$, the survival probability $\Psi^S(t)$ is equal to $\Psi^S(t) = \int_t^\infty \psi^S(\tau')d\tau'$. When $P_S < 1$, we use the subordination theory to find the survival probability

$$\Psi(t) = \sum_{n=0}^{\infty} \int_0^t \psi_n^{(S)}(t')(1-P_S)^n \, \Psi^{(S)}(t-t')dt' \qquad (A.1)$$

Now, we need to apply the Laplace transformation on Eq. A.1 to determine $\hat{\Psi}^S(u)$. In order to do the transformation, the analysis on each term in as follows: using the time convolution theorem, we can write the

$$\psi_n^{(S)}(t) = \int_0^t \psi_{n-1}^{(S)}(t') \, \psi_1^{(S)}(t-t')dt' \qquad (A.2)$$

Applying the Laplace transform on Eq. A.2, we obtain

$$\psi_n^{(S)}(u) = \psi_{n-1}^{(S)}(u) \, \psi_1^{(S)}(u) \qquad (A.3)$$

Note that $\psi_1^{(S)}(t) = \psi(t)$ and $\psi_0^{(S)}(t) = \delta(t)$. Thus $\hat{\psi}_n^{(S)}(u) = \left(\hat{\psi}^S(u)\right)^n$.

On the other hand, in order to apply the Laplace transform on $\Psi^{(S)}(t-t')$, we used the definition of $\Psi^{(S)}(t) = 1 - \int_0^t \psi^{(S)}(t')dt'$ and then apply the Laplace transform and we arrive at $\hat{\Psi}^S(u) = 1/u\left(1-\hat{\psi}^S(u)\right)$. Therefore, after applying the Laplace transform on Eq. A.1 we get

$$\hat{\Psi}(u) = \frac{1}{u}\left(1-\hat{\psi}^S(u)\right)\sum_{n=0}^{\infty}\left(\hat{\psi}^S(u)\right)^n (1-P_S)^n \qquad (A.4)$$

Using the geometric series properties, Eq. A.4 reads as

$$\hat{\Psi}^S(u) = \frac{1}{u} \, \frac{1-\hat{\psi}^S(u)}{1-\hat{\psi}^S(u)(1-P_S)} \qquad (A.5)$$

Dividing Eq. A.5 by $1-\hat{\psi}^S(u)$ and introducing $\hat{\Phi}(u) = \frac{u\hat{\psi}^S(u)}{1-\hat{\psi}^S(u)}$, we arrive at Eq. 2.7.

APPENDIX B

TIME CONVOLUTION OF SURVIVAL PROBABILITY

Let us define

$$\hat{p}(x,u/x_0) = \int_0^\infty e^{-ut}\, p(x,t/x_0)dt \qquad (B.1)$$

And

$$\hat{p}(x,u/\Theta) = \int_0^\infty e^{-ut}\, p(x,t/\Theta)dt \qquad (B.2)$$

And the Laplace transform of survival probability, $\widehat{\Psi}(u) \equiv \int_0^\infty dt\, \Psi(t)\exp(-ut)$, we can used the convoluted nature of Eq. 3.11 we obtain

$$\hat{p}(x,u/x_0) = \hat{\psi}(u)\hat{p}(x,u/\Theta) \qquad (B.3)$$

Where

$$\hat{\psi}(u) = \frac{\hat{p}(x,u/x_0)}{\hat{p}(x,u/\Theta)} \qquad (B.4)$$

From [38] we have

$$\int_0^\infty e^{-ut}\frac{1}{\sqrt{\pi t}}\exp\left(-\frac{k^2}{4t}\right) = \frac{1}{\sqrt{u}}e^{-k\sqrt{u}} \qquad (B.5)$$

We get

$$\hat{p}(x,u/x_0) = \frac{1}{\sqrt{4D}}\; exp\left[\frac{S(x-x_0)}{2D}\right]\frac{exp\left[-\frac{x-x_0}{2D}\sqrt{2(u-c)}\right]}{\sqrt{u-c}} \qquad (B.6)$$

And

$$\hat{p}(x,u/\Theta) = \frac{1}{\sqrt{4D}}\; exp\left[\frac{S(x-\Theta)}{2D}\right]\frac{exp\left[-\frac{x-\Theta}{2D}\sqrt{2(u-c)}\right]}{\sqrt{u-c}} \qquad (B.7)$$

With $C = -\frac{S^2}{4D}$. Thus using Eqs. B.6 and B.7 and plugging into Eq. B.4, we arrive at

$$\hat{\psi}(u) = exp\left\{\frac{\Theta - x_0}{2D}\left[S - (S^2 + 4Du)^{1/2}\right]\right\} \qquad (B.8)$$

Let us use [38]

$$\int_0^{\infty} e^{-ut} \frac{1}{\sqrt{\pi t^3}} exp\left(-\frac{k^2}{4t}\right) dt = e^{-k\sqrt{u}} \ , \ k \geq 0 \qquad (B.9)$$

This allows us to apply anti-Laplace transform on Eq. B.8 and obtain the result of Eq. 3.12.

BIBLIOGRAPHY

[1] P. Sibani, H. J. Jensen, World Scientific and Imperial College Press, ISBN 978-1-84816-993-7 (2013) .

[2] N. Boccara, Springer-Verlag, ISBN 0-387-40462-7, (2004).

[3] R. W. Sperry, Neuroscience **5**, 195-206 (1980).

[4] E. Tagliazucchi, D.H. Chialvo, Studies of Nonlinear Phenomena in Life Science **15**, 57-80 (2011).

[5] T. W. Robbins, Neuropsychopharmacology 36(1), 1–2 (2011).

[6] P. Bak, C. Tang, K. Wiesenfeld, Phys. Rev. Lett. **59**, 381-384 (1987).

[7] P. Lansky, S. Ditlevsen, BioCybern, 99:235 (2008).

[8] J. M. Beggs, D. Plenz, J. Neurosci, **23**, 11167-11177 (2003

[9] F. Lombardi, H. J. Herrmann, C. Perrone-Capano, D. Plenz, L. de Arcangelis, Phys. Rev. Lett. **108**, 228703, 1-5 (2012).

[10] W. L. Shew, D. Plenz, The Neuroscientist, **19**, 88-100 (2012).

[11] C. Haldeman, J. M. Beggs, Phys. Rev. Lett. **94**, 058101, 1-4 (2005).

[12] J. E. S. Socolar, S. A. Kauffman, Phys. Rev. Lett. **90**, 068702, 1-4 (2003).

[13] W. L. Shew, H.Yang, S. Yu, R. Roy, D. Plenz, J. Neurosci. 31, 55-63 (2011).

[14] D. B. Larremore, W. L. Shew, E. Ott, J. G. Restrepo, Chaos **21**, 025117, 1-10 (2011).

[15] N. Bertschinger, T. Natschlager, Neural. Comput. **16**, 1413-1436 (2004).

[16] D. Plenz, T. C.Thiagarajan, Trends Neurosci, **30**, 101-110 (2007).

[17] J. M. Beggs, Phil. Trans. R. Soc. A **366**, 329-343 (2008).

[18] D. R. Chialvo, Physica A **340**, 756-765 (2004).

[19] D. R. Chialvo, Nat. Phys. **6**, 744-750 (2010).

[20] J. P Onnela, J. Saramaki, J. Hyvonen, G, Szabo, D. Lazer ,K, Kaski, J. Kertesz, A. L. Barabasi, Proceedings of the National Academy of Sciences 104 (18): 7332–7336(2007).

[21] G. Werner, Chaos, Solitons and Fractals, in press (2013).

[22] K. G. Wilson, J. Kogut, Phys. Rep. **12**, 75-199 (1974).

[23] N. Dehghani, N. G. Hatsopoulos, Z. D. Haga, R. A. Parker, B. Greger, E. Halgren, S. S. Cash, A. Destexhe, Front. Physiol. **3**, 302, 1-18 (2012).

[24] R. Metzler,J. Klafter, Journal of Non-Crystalline Solids **305**, 81 (2002).

[25] West, B.J., Bologna, M., Grigolini, P, Springer-Verlag, New York (2003).

[26] S. Bianco, M. Ignaccolo, M.S. Rider, M.J. Ross, P. Winsor, P. Grigolini, Phys. Rev. E, **75**, 061911 (2007).

[27] R. Failla, M. Ignaccolo, P, Grigolini, A. Schwettmann, Phys. Rev E, **70**, 010101 (2004).

[28] A.-L. Barabási, Nature, **435**, 207-211 (2005).

[29] I.M. Sokolov, Phys. Rev. E, **63**, 011104; (2000)

[30] E. Barkai, R.J. Silbey, J. Phys. Chem. B, **104**, 3866 (2000).

[31] R. Metzler, J. Klafter, J.Phys. Chem. B, **104**, 3851 (2000).

[32] I.M. Sokolov, J. Klafter, Chaos, **15**, 026103 (2005).

[33] D. Plenz and T. C. Thiagarajan, Trends in Neurosciences, **30**, 101 (2007).

[34] C. S. Peskin, New York University, New York, 268-278, 1975.

[35] R. E. Mirollo, S. H. Strogatz, SIAM journal of applied mathematics, **50**, 1645-1662 (1990).

[36] E. Geneston, P. Grigolini, World Scientific, Studies of Nonlinear Phenomena in LifeScience, Singapore,Vol.**15**, 135–160 (2011).

[37] L. P. Kadanoff, World Scientific. ISBN 981-02-3764-2 (2000).

[38] M. Abramowitz, I. A. Stegun, Dover Publication, New York (1965).

[39] H. A. Kramers, Physica **7**, 284 (1940).

[40] B.J. Kim, Phys. Rev. Lett., **93**, 168701 (2004).

[41] M. Turalska, E. Geneston, B.J. West, P. Allegrini, P. Grigolini, Front. Physiol, **3**, 52 (2012).

[42] M.I. Ham, L. M.A. Bettencourt, F.D. McDaniel, G.W. Gross, Journal of Computational Neuroscience, **24**, 346-357 (2008).

[43] E. Lovecchio, P. Allegrini, E. Geneston, B. J.West, P. Grigolini, Front. Physiol. **3**, 96 (1-9) (2012).

[44] G. W. Gross, Multielectrode arrays, Scholarpedia, **6**(3):5749(2011).

[45] E. Niedermeyer, F.L. da Silva, Lippincot Williams & Wilkins. ISBN 0-7817-5126-8(2004).

[46] P. Grigolini, M. Zare, A. Svenkeson, B. J. West, edited by D. Plenz and E. Niebur, (eds.) John Wiley & Sons,New York ISBN: 978-3-527-41104-7 (2013).

[47] G. Longo, M. Montevil, Front. Physiol, **3**: 39, (2012).

[48] K. Binder, Z. Phys. B. **43**, 119-140 (1981).

[49] M. Turalska, B. J. West, P. Grigolini, Sci. Rep. **3**,1371 (1-8) (2012).

[50] M. Turalska, B. J. West, P. Grigolini, Phys. Rev. E **83**, 061142 (1-6) (2011).

[51] I. Podlubny, M. Kacenak, MATLAB Central File Exchange, File ID 8735, mlf.m, http://www.mathworks.com/matlabcentral/fileexchange (2005).

[52] A. Svenkeson, M. Bologna, P. Grigolini, Phys. Rev. E **86**, 041145 (1-10) (2012).

[53] Y. F. Contoyiannis, F. K. Diakonos, Phys. Lett. A **268**, 286-292 (2000); Y. F. Contoyiannis, F. K. Diakonos, A. Malakis, Phys. Rev. Lett. **89**, 035701 (1-4) (2002).

[54] S. Bianco, P. Grigolini, P. Paradisi, J. Chem. Phys. **123**, 174704 (1-10) (2005).

[55] J. L. Rodgers, W. A. Nicewander, The American Statistician, **42**, 5966 (1988).

[56] A. Kraskov, H. Stogbauer, R. G. Andrzejak, P. Grassberger, Europhys. Lett. **70**, 278-284 (2005).

[57] S. Zapperi, K. B. Lauritsen, H.E. Stanley, Phys. Rev. Lett. **75**, 4071-4074 (1995).

[58] V. Priesemann, M. H. J. Munk, M. Wibral, BMC neuroscience, **10**, 40 (1-20) (2009).

[59] J. M. Beggs, N. Timme, Front. Physiol. **3**, 163 (1-14) (2012).

[60] J. Touboul, A. Destexhe, PLoS ONE **5**, 8982 (1-14) (2010).

[61] S. Luccioli and A. Politi, Phys. Rev. Lett. **105**, 158104 (2010).

[62] K. Christensen, N. R. Moloney, Imperial College Press, London, 2005.

[63] F. Mainardi, J. Comp. Appl. Math. **118**, 283 (2000).

[64] N. Korabel, E. Barkai, Phys. Rev. Lett. **108**, 060604 (2012).

[65] S. Burov, R. Metzler, E. Barkai, Proc. Natl. Acad. Sci. USA **107**, 13228 (2010).

[66] F. Vanni, M. Lukovic, P. Grigolini, Phys. Rev. Lett. **107**, 078103 (2011).

[67] A. R. Bulsara, T. C. Elston, C. R. Doering, S. B. Lowen, K. Lindenberg, Phys. Rev. E **53**, 3958 (1996).

[68] P. L´ansk´y, Phys. Rev. E **55**, 2040 (1997).

[69] M. Zare, P. Grigolini, Phys. Rev. E **86**, 051918 (1-6) (2012).

[70] L. de Arcangelis, C. Perrone-Capano, and H. J. Herrmann, Phys. Rev. Lett. **96**, 028107 (2006).

[71] L. de Arcangelis, Eur. Phys. J. Special Topics **205**, 243 (2012).

[72] V. F. Pisarenko and D. Sornette, Eur. Phys. J. Special Topics **205**, 95 (2012).

[73] M. Turalska, E. Geneston, B. J. West, P. Allegrini, P. Grigolini, Front. Physiol **3**, 52 1-6 (2012).

[74] D. Fulger, E. Scalas, G. Germano, Phys. Rev. E **77**, 021122 (1-7) (2008).

[75] R. Bettin, R. Mannella, B. J. West, P. Grigolini, Phys. Rev. E **51**, 212-219 (1995).

[76] E. Floriani, R. Mannella, P. Grigolini, Phys. Rev. E **52**, 5910-5917 (1995).

[77] Y. Pomeau, P. Manneville, Comm. Math. Phys. **74**, 189-197 (1980).

[78] S. Boccaletti, V. Latora, Y. Moreno, M. Chavez, D.-U. Hwang, Phys. Rep. **424**, 175–308 (2006).

[79] A. Arenas ,A. Díaz-Guilera ,J. Kurths, Y. Moreno, C. Zhou, Phys.Rep. **469**,93–153 (2006).

[80] D.O. Hebb, Organization of Behavior, New York: Wiley (1949).

[81] D. Fraiman, P.Balenzuela, J. Foss, D.R. Chialvo, Phys.Rev.E **79**, 061922 (2009).

[82] N. W. Hollingshad, M. Turalska, P. Allegrini; B. J. West, P. Grigolini, Physica A **391**, 1894-1899 (2012).

[83] R. Cohen, S. Havlin, Phys. Rev. Lett. **90**, 1–4 (2003).

[84] W. Gao, J. H. Gilmore, K. S. Giovanello, J. K. Smith, D. Shen, H. Zhu, W. Lin, PLoS ONE **6**(9): e25278 (2011). doi:10.1371/journal.pone.0025278.